

## **Supplementary Materials**

### **Histological validation of atrial structural remodelling in patients with atrial fibrillation**

**Yuya Takahashi, Takanori Yamaguchi et al.**

## **Index**

Definition of types of AF and heart failure, and other information	5
Electroanatomic mapping	6
Catheter ablation and follow-up	8
Atrial tissue sampling and processing for histology	9
Quantification of histological factors on light microscopy	10
Tissue preparation and evaluation by electron microscopy	12
Analysis of inflammatory cell infiltration	13
Statistical analysis	14
Validation and advantages of the 1 cm <sup>2</sup> -area method	17
Additional data indicating that voltage reduction is a diffuse process	18
Supplementary Table S1	19
Supplementary Table S2	21
Supplementary Table S3	23
Supplementary Table S4	25
Supplementary Table S5	27
Supplementary Table S6	28
Supplementary Table S7	29
Supplementary Table S8	30
Supplementary Table S9	31
Supplementary Table S10	32
Supplementary Table S11	33
Supplementary Table S12	34

Supplementary Table S13	35
Supplementary Table S14	36
Supplementary Figure S1	37
Supplementary Figure S2	38
Supplementary Figure S3	39
Supplementary Figure S4	40
Supplementary Figure S5	41
Supplementary Figure S6	42
Supplementary Figure S7	43
Supplementary Figure S8	44
Supplementary Figure S9	45
Supplementary Figure S10	46
Supplementary Figure S11	47
Supplementary Figure S12	48
Supplementary Figure S13	49
Supplementary Figure S14	50
Supplementary Figure S15	51
Supplementary Figure S16	52
Supplementary Figure S17	53
Supplementary Figure S18	54
Supplementary Figure S19	55
Supplementary Figure S20	56



## **Definition of AF type**

Atrial fibrillation (AF) was classified as paroxysmal AF (PAF), defined as AF that terminates spontaneously or with intervention within 7 days of onset; persistent AF, defined as continuous AF that is sustained beyond 7 days; or long-standing persistent AF, defined as continuous AF of greater than 12 months duration.<sup>1</sup>

## **Definition of heart failure**

Patients with a history of heart failure (HF) were classified as follows according to the left ventricular ejection fraction (LVEF) at HF diagnosis: reduced LVEF (<40%), mid-range LVEF (40-49%), or preserved LVEF ( $\geq$ 50%).

## **Other information**

### **Computed tomography**

All patients underwent transthoracic echocardiography and contrast-enhanced computed tomography (CT) before ablation to evaluate the left atrium (LA) volume. Patients with reduced renal function underwent CT without contrast. The LA volume divided by body surface area (BSA) was expressed as the LA volume/BSA.

### **Control group**

Patients in the control group underwent transthoracic echocardiography only.

### **Antiarrhythmic drugs**

Antiarrhythmic drugs, with the exception of amiodarone, were discontinued for at least five half-lives before ablation.

## **Electroanatomic mapping**

### **Voltage mapping**

The details of voltage mapping have been described previously.<sup>2</sup> In brief, a three-dimensional (3D) geometry and high-density bipolar voltage map of the right atrium (RA) septum and entire LA were created during high RA pacing at 600 ms cycle length using a 3D-electroanatomical mapping system (EnSite Precision™, Abbott, St. Paul, MN, USA) and GMC (Advisor™ HD Grid, Abbott). The bipolar voltage is defined as the peak-to-peak electrogram amplitude. All bipolar signals were collected along and across GMC splines, with only the highest amplitude (along vs. across) bipolar signal displayed on the voltage map in order to minimize the impact of directional sensitivity.<sup>2,3</sup> Premature atrial beats were excluded. The maximum distance between the mapping points was set to 5 mm. The bipolar electrograms were filtered using a bandpass filter (30–500 Hz). At the beginning of the procedure, the patients underwent biphasic direct current cardioversion (DC) to restore sinus rhythm (SR). If an external DC  $\geq 270$  J failed to restore SR, pulmonary vein isolation (PVI) was established during AF, followed by cardioversion. Subsequently, a voltage map was created.

### **Definition of the low-voltage area and electrical scar**

Low-voltage area (LVA) was defined as an area with bipolar voltage  $< 0.5$  mV and  $\geq 3.0$  cm<sup>2</sup>. Electrical scar was defined as an area with bipolar voltage  $< 0.05$  mV and  $\geq 1.0$  cm<sup>2</sup>. The presence of LVA and electrical scar were evaluated at the biopsy site and in the whole LA excluding pulmonary veins and left atrial appendage.

### **Evaluation of global LA voltage ( $V_{GLA}$ ) and regional LA voltage ( $V_{RLA}$ )**

The LA surface was subdivided into areas of 1.0 cm<sup>2</sup>, and the highest voltage in each area was manually acquired. Then, the global LA voltage ( $V_{GLA}$ ) was calculated as the mean of the highest voltages in each 1.0 cm<sup>2</sup> area over the entire LA (1 cm<sup>2</sup>-area method), excluding the following regions: left atrial appendage (LAA), LA ridge between the pulmonary veins (PVs) and the LAA, PVs at the ostium level, and the mitral annular region defined as a region  $\leq 10$  mm of the atrial side from the minimum atrial electrogram recording site<sup>2</sup> (Supplementary Material, *Figure S1*).

The LA was subdivided into six anatomical regions, including the anterior, septal, roof, inferior, posterior, and lateral regions. Regional LA voltage ( $V_{RLA}$ ) according to the six anatomical regions was also calculated as the mean of the highest voltage in each 1 cm<sup>2</sup> area (Supplementary Material, *Figure S1*). The details of the method for subdividing the LA into six regions have been previously described.<sup>2</sup>

### **Evaluation of voltage at biopsy site ( $V_{biopsy}$ )**

The biopsy site was annotated on the 3D geometry using the GMC and was defined as a 1.5 cm x 1.0 cm area.<sup>2</sup> To evaluate voltage at the biopsy site ( $V_{\text{biopsy}}$ ), the area was subdivided into six areas of 0.25 cm<sup>2</sup>.<sup>2</sup> The highest voltage in each area was manually acquired and  $V_{\text{biopsy}}$  was calculated as the mean of the six highest voltages (Supplementary Material, *Figure S1*). Because biopsies were sometimes performed at two locations about 1 cm apart, as described in ‘atrial tissue sampling and processing for histology’ in the Supplementary Material, *Appendix*, the 1.5 cm<sup>2</sup> area was defined as the biopsy site. As with the evaluation of  $V_{\text{GLA}}$ , calculating the mean value of the voltage at a sampling density of 1 cm<sup>2</sup> at the biopsy site (i.e., the mean of two points) may not accurately evaluate the mean value of the biopsy site. Therefore, we evaluated  $V_{\text{biopsy}}$  with a sampling density of 0.25 cm<sup>2</sup>, although the sampling density was different from the evaluation of  $V_{\text{GLA}}$ .

### **Analysis of the proportion of fractionated electrograms**

Fractionated atrial electrograms were evaluated using the electroanatomic map created during high RA pacing. The fractionation mapping tool of EnSite Precision<sup>TM</sup> mapping system was used. Fractionated electrograms were defined as  $\geq 5$  deflections in each electrogram counted based on the following detection criteria: peak-to-peak voltage (sensitivity) of  $>0.04$  mV, width of 5 ms, and refractory of 6 ms. Sensitivity means the minimum voltage amplitude required for a deflection to register as a fractionation. Width means the maximum time allowed from the start of deflection until return to the isoelectric baseline to count one fractionation. Refractory means the minimum time allowed from start of one fractionation until a second fractionation may be counted.<sup>4</sup> The proportion of points with fractionated electrograms to all mapping points in the LA was calculated as %Fractionated EGM. The proportion of fractionated electrograms at the biopsy site was also evaluated.

### **Analysis of local slow conduction zones**

The presence of a slow conduction zone (SCZ), defined as  $< 30$  cm/s,<sup>5</sup> was assessed by using an isochronal activation map created during high RA pacing. The method of analyzing SCZs is shown in Supplementary Figure S2. Isochronal activation maps were created using the EnSite AutoMap module. The interval between color bars was set to 95 ms, which was divided into 7 segments (8 colours from white to purple). Each isochrone corresponds to 13.6 ms. Tags with a diameter of 4 mm were used; when one or more isochrones were identified in a 4 mm tag, the conduction velocity across the 4 mm tags was calculated as 29 cm/s. When the width of the SCZ was 20 mm or more, it was considered as a local SCZ. The number and total width of the SCZs ( $\text{SCZ}_{\text{total}}$ ) in the LA were calculated. SCZs along the PV ostium or inside the PVs were excluded from the analysis. The presence of SCZs was also assessed at the biopsy site.

## **Catheter ablation and follow-up**

PVI was performed in all patients using a contact force-sensing catheter (TactiCath Quartz<sup>TM</sup>; Abbott). After PVI, atrial burst pacing from the coronary sinus until 2:1 atrial capture was performed to induce LA macroreentrant tachycardia (LAMRT) and cavotricuspid isthmus-dependent atrial flutter before and after a bolus injection of 10 µg isoproterenol. LAMRT was defined as a cycle length of > 180 ms that lasted > 5 min, and the reentrant circuit was confirmed by electroanatomic mapping and/or post-pacing interval mapping in the LA.<sup>2</sup> The critical isthmus was defined as the narrowest isthmus and the most crowded isochronal zone on the activation map.

When an LAMRT was induced, focal ablation at the critical isthmus which was usually located in the low-voltage area (LVA) defined as <0.5 mV was performed and subsequent linear ablation along the LVA was added when necessary.<sup>2</sup> When second or third LAMRT or biatrial tachycardia was induced, additional linear ablation was added.<sup>2</sup> When cavotricuspid isthmus-dependent atrial flutter was induced, linear ablation at the cavotricuspid isthmus was added. Finally, focal atrial tachycardia and non-PV ectopy-triggering AF were ablated when it was induced before or after isoproterenol infusion.

Follow-up was performed at 1, 3, and 6 months and then every 6 months using 12-lead ECG at each follow-up visit. 24-h Holter monitoring was performed at 12 months. As described in the consensus statement,<sup>1</sup> atrial tachyarrhythmia recurrence was defined as recorded on ECG or was otherwise documented to last for at least 30 s beyond a 3-month blanking period after the procedure. Transthoracic echocardiography was performed at the 12-month follow-up visit. Antiarrhythmic medications and anticoagulants were managed according to physician preference and current guidelines.



### **Atrial tissue sampling and processing for histology**

An atrial biopsy was performed before the transseptal puncture. Intracardiac echocardiography (ICE, ViewFlex™, Abbott, St. Paul, MN, USA) was performed in the RA to observe the long-axis view of the posterior part of the atrial septum at the position where the fossa ovalis (FO) and the limbus of FO were observed (Supplementary Material, *Figure S3A and 3B*). Then, a bioptome (5.5 Fr, 104 cm with a 2.46 mm<sup>3</sup> tip or 7.0 Fr, 104 cm with a 5.20 mm<sup>3</sup> tip; Cordis, Miami Lakes, FL) was advanced to the RA septum through a steerable sheath (Agilis, Abbott) and biopsy was performed at the posterior portion of the limbus of FO. Fluoroscopy was also used to confirm the rough location of the bioptome and the opening of the bioptome in the left anterior oblique view (LAO; Supplementary Material, *Figure S3C*). Because the atrial endocardium is thick, the initial biopsy usually contains only endocardial tissue (Supplementary Material, *Figure S3D*). The average thickness of the atrial endocardium in the region corresponding to the biopsy site was an average of 0.85 mm in the eight autopsy cases (Supplementary Material, *Figure S6 and Table S14*). Subsequent biopsies were targeted to the same site as the initial biopsy to increase the possibility of obtaining the myocardial tissue. No further biopsies were repeated at the same site if the biopsy specimen floated in 4% paraformaldehyde solution, suggesting that the bioptome had reached the adipose tissue deep in the atrial septum. In such cases, subsequent biopsies were performed at a site approximately 1 cm superior. Five samples ranging in size from 1 to 3 mm were obtained for each patient. At least three samples apparently containing myocardial tissue were immediately fixed in 4% paraformaldehyde solution for 48 h at 4°C. The remaining samples were cryopreserved for future analysis. To observe complications, the biopsy site was monitored using ICE during the ablation procedure.

## Quantification of histological factors on light microscopy

The embedded paraffin blocks were sectioned at 5  $\mu\text{m}$  thickness, and deparaffinized sections were stained with hematoxylin and eosin (H&E), Masson's trichrome, and Congo red. Staining was performed using the same protocol.

Each stained slide was scanned using a digital slide scanner (NanoZoomer S60, Hamamatsu, Japan) and the NDP.scan software (version 3.2.15). Quantitative analysis was performed using an image analysis platform (HALO version 2.3.2089.34; Indica Labs, Corrales, NM, USA). To determine the area for quantitative analysis, the edges of all myocardial tissues on the glass slides were manually annotated after excluding endocardial connective tissue and large adipose tissue outside the myocardial tissue. Sufficient myocardial tissue samples were defined as a total analysis area of  $\geq 100,000 \mu\text{m}^2$  (Figure 1 and Supplementary Material, *Figure S4*). Myocardial tissue with crush artifacts and contraction bands was excluded from the analysis whenever possible (Supplementary Material, *Figure S4*).

To determine the histological factors potentially associated with electroanatomic characteristics, the following parameters were quantitatively analyzed in all analysis areas based on Masson's trichrome staining: extent of fibrosis, including perivascular and interstitial fibrosis (%Fibrosis), intercellular space extent (%Intercellular space), myofibrillar loss severity (%Myofibrillar loss), and adipocyte extent (%Adipocytes) (Figures 1B–1E). Additionally, myocyte size and myocardial nuclear density were quantitatively analyzed by H&E staining (Figures 1F and 1G). Myocyte disarray was semi-quantitatively analyzed and classified as minimal (0), mild (1), moderate (2), or severe (3) (Figure 1H). Amyloid deposition was identified by Congo red staining and apple-green birefringence under a polarizing microscope (Figure 1I). Patients with amyloid deposition were analyzed separately from the amyloid group ( $n=12$ ) because of the difficulty in histological quantification resulting from advanced tissue damage.

For the measurement of %Fibrosis, the blue-stained areas from Masson's trichrome staining are highlighted in red, and the red area was divided by the analysis area (Figure 1B). %Intercellular space was calculated by manually tracing all interstitial regions in the analysis area (including blood vessels), subtracting the fibrotic areas, and finally dividing by the analysis area (Figure 1C). The percentage of myofibrillar loss was measured as follows: (1) all interstitial regions and adipocytes within the analysis area were manually excluded based on Masson's trichrome staining, and only myocytes were selected; (2) the contrast was adjusted such that the area of myofibrils stained darkest red-purple (highest staining density) accounted for 3% of the total myocyte area and was used as the upper limit reference (100%); and (3) areas of contrast less than 50% of the reference (calculated automatically) were defined as myofibrillar loss areas, and the percentage of that area from the total myocardial area was calculated (Figure 1D). The %Adipocytes was calculated by manually tracing all adipocyte regions and dividing that

area by the analysis area (Figure 1E). Myocyte size was evaluated using H&E staining and was defined as the maximum short diameter at the level crossing the nucleus (mean of  $\geq 50$  cardiomyocyte samples) (Figure 1F). The normal range of myocardial size is reported to be 6-12  $\mu\text{m}$ .<sup>6</sup> In this study, myocardial specimens with an average size  $>12 \mu\text{m}$  were defined as hypertrophic. The number of myocardial nuclei per analysis area was counted as nuclear density (Figure 1G), which was used as a substitute for myocyte cell number.<sup>7</sup> Nuclear size was defined as the maximum short diameter of the nucleus and was evaluated in 100 patients. Histological evaluation was performed by two observers who were blinded to clinical information and bipolar voltages. The samples were then reviewed by a pathologist.

## **Tissue preparation and evaluation by electron microscopy**

A single atrial sample was examined by transmission electron microscopy in 40 patients,<sup>8</sup> seven of whom had no cardiomyocytes observed and were excluded from the analysis. The sample was fixed in phosphate-buffered 2% glutaraldehyde and subsequently post-fixed in 2% osmium tetra-oxide for 3 h in an ice bath. The specimens were then dehydrated in graded ethanol and embedded in epoxy resin. Ultrathin sections were obtained by using an ultramicrotome. Ultrathin sections stained with uranyl acetate for 10 min and lead staining solution for 5 min were subjected to transmission electron microscopy observation (JEOL JEM1400FLASH at 100 kV). In the first 19 cases, the ultrastructure was evaluated mainly in the myocardial parenchyma at a minimum of 10 sites in each patient, while in the latter 14 cases, each case was analyzed at five randomly designated parenchymal and five interstitial sites (Supplementary Material, *Figure S5*).

Ultrastructural changes, including interstitial structure, myofilament changes, mitochondrial abnormalities (size, shape, and number), glycogen granules, and autophagic vacuoles, were classified as positive or negative. To compare the signal intensity of the plasma components in the capillaries with areas without obvious structures within the increased intercellular spaces, the mean gray value within the selected area was measured using ImageJ (Ver. 1.50b, National Institutes of Health, Bethesda, USA) (Figure 3). Myofilament changes were semi-quantitatively classified as no or minimal myofilament lysis (0), mild myofilament lysis (1), moderate myofilament lysis (2), or severe myofilament lysis (3) (Figure 4). The electron microscopy findings for biopsied samples were evaluated by three observers (T.S., T.Y., and Y.T.) who were blinded to the clinical background of the patients, with each sample examined three times in random order.

## **Analysis of inflammatory cell infiltration**

### **Immunohistochemical staining**

Immunohistochemistry of paraformaldehyde-fixed paraffin-embedded sections was performed manually. Commercially available antibodies were used as primary antibodies to detect inflammatory cell infiltrates, including CD3 (413241, Nichirei, not diluted) for T lymphocytes, CD20 (IR604, DAKO, not diluted) for B lymphocytes, CD45 (422071, Nichirei, not diluted) for leukocyte common antigen (all nucleated hematopoietic cells), CD11c (AMAb90915, AAB, 1:200) for M1 macrophages, and CD163 (HPA046404, AAB, 1:300) for M2 macrophages, with an incubation time of 60 min at room temperature. For detection, a biotin-free, horseradish peroxidase labeled polymer complex conjugated with a secondary antibody (K4061, Dako, EnVision plus Dual Link System-HRP) was used with an incubation time of 60 min at room temperature. Samples obtained from the human tonsils were used as positive controls for the corresponding antibodies.

### **Counting of the inflammatory cell infiltrates**

The number of infiltrating CD3-, CD20-, CD45-, CD11c-, and CD163-positive cells in the entire analysis area was counted by two observers following blinding protocol. Positive cells in the vessels were excluded from the total count. The cell number was then divided by the analysis area to be expressed as the number of cells/mm<sup>2</sup>.

## Statistical analysis

### Categorization of the AF groups based on $V_{GLA}$

Patients in the AF group were classified into quartiles (Q1–Q4) based on the  $V_{GLA}$ . Baseline characteristics and electroanatomic data were compared across quartiles using trend tests, in which Spearman's rank correlation coefficient and the Cochran-Armitage test were used for continuous and categorical data, respectively.

### Multiple linear regression analysis

Histological factors associated with each electroanatomic characteristic ( $V_{GLA}$ ,  $V_{biopsy}$ , %Fractionated EGM, and  $SCZ_{total}$ ) in the AF group were analyzed using multiple linear regression. Because the distribution of %Fractionated EGM was non-normally distributed, it was log-transformed and normalized before multiple regression analyses. The distribution of  $SCZ_{total}$  was not continuous because we counted and measured the total width of the SCZs only if the width of each SCZ was 20 mm or more. Therefore, we converted  $SCZ < 20$  mm to 1,  $SCZ_{total} \geq 20$  and  $< 40$  to 2,  $SCZ_{total} \geq 40$  and  $< 60$  to 3, and thereafter to continuous values of up to 24 at intervals of 20 mm each. Because the continuous data were non-normally distributed, they were log-transformed and normalized. Using histological factors as independent variables (%Fibrosis, %Intercellular space, %Myofibrillar loss, %Adipocyte, myocyte size, nuclear density, and myocyte disarray), we identified histological factors significantly associated with each electroanatomic characteristic (Table 2).

Clinical factors significantly associated with each electroanatomic characteristic ( $V_{GLA}$ ,  $V_{biopsy}$ , %Fractionated EGM, and  $SCZ_{total}$ ) were identified using multiple linear regression analysis. In this analysis, normalized data were used for %Fractionated EGM and  $SCZ_{total}$  as described above. Age, female sex, BSA, history of heart failure, hypertension, diabetes mellitus, PeAF/LS-PeAF type, LA volume/BSA, and LV ejection fraction were selected as independent variables.

Clinical factors significantly associated with each histological factor (%Fibrosis, %Intercellular space, %Myofibrillar loss, and nuclear density) were identified using multiple linear regression analysis. Age, female sex, BSA, history of heart failure, hypertension, diabetes mellitus, PeAF/LS-PeAF type, LA volume/BSA, and LV ejection fraction were selected as independent variables.

Finally, using the clinical factors associated with  $V_{GLA}$  as covariates (age, BSA, female sex, LA volume/BSA, and PeAF/LS-PeAF type), histological factors that were significantly associated with each electroanatomic characteristic were identified with covariate adjustment.

In the multiple regression analyses, the  $p$  value was adjusted using the Benjamini-Hochberg

(BH) method.

To identify which of the four histological factors were associated with voltage in the Q1 or Q2–Q4 categories, multiple linear regression analyses were separately performed in the Q1 and Q2–Q4 categories.

### **Linear mixed-effects model**

$V_{GLA}$  may lose local/regional voltage information. Therefore, we created the linear mixed-effects model with all voltage data (mean  $1,339 \pm 377$  acquired points per patient) as a dependent variable. The seven histological factors were used as fixed factors and patient ID as random effects. The  $p$  value was adjusted using the Benjamini-Hochberg (BH) method.

### **Comparison of histological factor or electroanatomic characteristics between AF types**

When comparing the four histological factors or electroanatomic characteristics between AF types (PAF, PeAF, and LS-PeAF), the Tukey-Kramer test was performed.

### **Comparison of electron density in the electron microscopy analysis**

The paired t-test was used to compare the electron densities of the intracapillary and interstitial plasma components in each patient.

### **Relationship between each histological factor and inflammatory cell infiltration**

To analyze the relationship between each histological factor and inflammatory cell infiltration, the cell numbers were compared between the two groups (high vs. low), divided by the median value of each histological factor in the AF group ( $n=230$ ). The  $p$  value was adjusted using the Benjamini-Hochberg (BH) method.

### **Atrial tachyarrhythmia recurrence**

To evaluate the relationship between atrial tachyarrhythmia recurrence and each histological or electroanatomic characteristic, patients were divided into two groups based on each cutoff value, and atrial tachyarrhythmia-free survival time was determined by Kaplan–Meier estimation and compared between groups using the log-rank test. Each cutoff value was determined using the Youden index based on recurrence in patients with a follow-up of more than 12 months ( $n=202$ ).

### **Inducibility of left atrial macroreentrant tachycardia**

To evaluate the discriminative power of each electroanatomic characteristic and histological factor for the inducibility of LAMRT, receiver operating curve (ROC) analysis was performed, and the area under the ROC curve (AUC) and 95% confidence interval (CI) were calculated.

### **Others**

To examine whether %Fibrosis differed between the RA septum and each LA region in the eight autopsy cases, the Friedman test was performed. Intraobserver and interobserver agreements for histological evaluation using light microscopy were calculated using the intraclass correlation coefficient (ICC) score for 29 randomly selected patients. The ICC (1, 1) and ICC (2, 1) for %Fibrosis were 0.955 and 0.891, respectively.



## **Validation and advantages of the 1 cm<sup>2</sup>-area method**

### **Validation of V<sub>GLA</sub>**

To validate the 1 cm<sup>2</sup>-area method, we also evaluated V<sub>GLA</sub> using all annotated points (all-annotated-point method),<sup>2</sup> in which all the voltage data annotated on the surface of the entire LA, excluding the PVs, LAA, and mitral annular region, were extracted from the intraoperative recordings in csv file format, and V<sub>GLA</sub> was calculated as the mean of all annotated points. Then, the V<sub>GLA</sub> obtained using the two methods were then compared. A comparison of V<sub>GLA</sub> between the 1 cm<sup>2</sup>-area method and the all-annotated-point method showed a strong positive correlation (Supplementary Material, *Figure S7*).

### **Advantages of the 1 cm<sup>2</sup>-area method**

The evaluation of V<sub>GLA</sub> by the 1 cm<sup>2</sup>-area method required approximately five minutes, whereas the all-annotated-point method required more than 30 minutes for each case on the current EnSite system, and analysis cannot be performed unless the EnSite system is closed once. The former is a more clinically feasible method; hence, the 1 cm<sup>2</sup>-area method was employed in this study.

## **Additional data indicating that voltage reduction is a diffuse process**

### **Analysis of $V_{RLA}$ in patients categorized into the Q1 or those with low-voltage area**

The  $V_{RLA}$  in all patients categorized in Q1 was lower than the mean  $V_{RLA}$  of the control groups in any LA region. All patients with low-voltage areas defined as  $<0.5$  mV identified in any of the LA regions had lower  $V_{RLA}$  compared to the mean  $V_{RLA}$  of the control group (Supplementary *Figure S8*), suggesting that the presence of LVA itself reflects a severe reduction in the global LA voltage and that voltage reduction is a diffuse process.

### **Analysis of the proportion of low-voltage electrograms**

We evaluated the proportion of low-voltage electrograms, defined as  $<0.5$  mV. First, all the voltage data annotated during HRA pacing on the surface of LA, excluding the PVs, LAA, and mitral annular region, were extracted from the intraoperative recordings in the csv file format.

Then, the proportion of low-voltage electrograms (%Low-voltage EGM)  $<0.5$  mV to all electrograms used on the voltage map was calculated. Similarly, we evaluated %Low-vol EGM  $<1.0$  mV and %Low-vol EGM  $<1.5$  mV.

The relationship between  $V_{GLA}$  and %Low-vol EGM is shown in Supplementary *Figure S9*. %Low-vol EGM defined as  $<0.5$  mV sharply increased as  $V_{GLA}$  decreased below 4.0 mV, showing that reduction in  $V_{GLA}$  is closely associated with an increase in low-voltage electrograms in the LA. Furthermore, %Low-vol EGM defined as  $<1.0$  mV and  $<1.5$  mV increased as  $V_{GLA}$  decreased below approximately 6.0 mV and 8.0 mV, respectively.

**Table S1. Patient characteristics included in the analysis as well as control**

Variables	Q1, <4.2 mV, n = 57	Q2, ≥4.3 <5.9 mV, n = 57	Q3, ≥6.0 <7.5 mV, n = 58	Q4, ≥7.6 mV n = 58	Control n = 26	<i>P</i> for trend in Q1–4	<i>P</i> value Q4 vs. control
Clinical parameters							
Age (range), years	75 ± 8 (44–91)	69 ± 10 (24–85)	64 ± 9 (39–83)	59 ± 14 (21–90)	54 ± 13 (20–76)	<0.001*	0.209
Female sex, n (%)	30 (53)	21 (37)	13 (22)	5 (9)	13 (50)	<0.001*	<0.001*
BSA, m <sup>2</sup>	1.62 ± 0.20	1.69 ± 0.18	1.74 ± 0.16	1.84 ± 0.19	1.77 ± 0.22	<0.001*	0.155
Underlying heart disease, n (%)	3 (5)	4 (7)	2 (3)	7 (13)	2 (8)	0.260	0.714
Ischemic cardiomyopathy	1 (2)	1 (2)	0 (0)	1 (2)	1 (4)	0.785	0.529
Dilated cardiomyopathy	0 (0)	0 (0)	2 (3)	3 (5)	0 (0)	0.027*	0.549
Hypertrophic cardiomyopathy	2 (4)	3 (5)	0 (0)	3 (5)	1 (4)	0.982	1.000
CHA <sub>2</sub> DS <sub>2</sub> -VASc, median (IQR)	4 (3–5)	2 (1–4)	2 (1–3)	2 (1–2)	1 (0–1)	<0.001*	0.004*
History of heart failure, n (%)	22 (39)	15 (26)	9 (16)	10 (17)	2 (8)	0.003*	0.326
HF <sub>r</sub> EF	7 (12)	9 (16)	2 (3)	4 (7)	1 (4)	0.101	1.000
HF <sub>mr</sub> EF	3 (5)	2 (4)	3 (5)	1 (2)	1 (4)	0.433	0.526
HF <sub>p</sub> EF	12 (21)	4 (7)	4 (7)	5 (9)	0 (0)	0.042*	0.318
Hypertension, n (%)	37 (65)	31 (54)	32 (55)	29 (50)	6 (23)	0.134	0.031*
Diabetes mellitus, n (%)	14 (25)	7 (12)	8 (14)	13 (22)	3 (12)	0.835	0.369
History of stroke, n (%)	6 (11)	8 (14)	2 (3)	3 (5)	0 (0)	0.101	0.549
eGFR, mL/min/1.73 m <sup>2</sup>	57 ± 16	61 ± 22	65 ± 12	67 ± 18	74 ± 13	<0.001*	0.084
AF type, n (%)							
PAF	16 (28)	17 (30)	22 (38)	31 (53)	–	0.003*	–
PeAF	20 (35)	16 (28)	22 (38)	19 (33)	–	0.917	–
LS-PeAF	20 (35)	24 (42)	14 (24)	8 (14)	–	0.002*	–
Medication at baseline, n (%)							
ACEi or ARB	24 (42)	21 (37)	19 (33)	22 (38)	3 (12)	0.563	0.019*
MRA	6 (11)	2 (4)	3 (5)	4 (7)	0 (0)	0.530	0.306

Diuretics (other than MRA)	12 (21)	8 (14)	3 (5)	7 (12)	0 (0)	0.072	0.094
Class I antiarrhythmic drugs	4 (7)	6 (11)	12 (21)	12 (21)	1 (4)	0.015*	0.056
Beta-blockers	35 (61)	36 (63)	28 (48)	20 (34)	7 (27)	0.001*	0.616
Amiodarone	11 (19)	4 (7)	2 (3)	2 (3)	0 (0)	0.002*	1.000
Bepridil	3 (5)	3 (5)	8 (14)	1 (2)	3 (12)	0.880	0.086
LA volume/BSA, mL/m <sup>2</sup>	112 ± 25	99 ± 23	90 ± 25	84 ± 26	–	<0.001*	–
LA diameter, mm	43 ± 5	42 ± 6	40 ± 6	41 ± 7	34 ± 6	0.010*	<0.001*
LV ejection fraction, %	61 ± 13	63 ± 11	63 ± 12	62 ± 12	63 ± 9	0.966	0.726
E/e'	11.7 ± 5.8	9.6 ± 2.9	8.1 ± 2.5	8.3 ± 3.4	6.3 ± 5.5	<0.001*	0.049*
Electroanatomic characteristics							
V <sub>biopsy</sub> , mV, median (IQR)	5.9 (4.8–6.8)	7.9 (5.9–9.9)	9.3 (7.4–10.8)	11.2 (8.9–13.3)	10.5 (7.5–12.1)	<0.001*	0.097
V <sub>GLA</sub> , mV, median (IQR)	3.4 (2.8–4.0)	5.1 (4.6–5.6)	6.8 (6.4–7.2)	8.6 (7.9–9.4)	8.3 (7.4–9.8)	<0.001*	0.433
LVA, n (%)	30 (53)	1 (2)	0 (0)	0 (0)	0 (0)	<0.001*	1.000
Scar, n (%)	3 (5)	0 (0)	0 (0)	0 (0)	0 (0)	0.019	1.000
%Fractionated EGM, %, median (IQR)	3.6 (2.3–6.2)	2.3 (1.1–3.5)	1.7 (1.0–3.0)	1.6 (1.3–2.3)	0.8 (0.3–1.5)	<0.001*	<0.001*
SCZ <sub>total</sub> , mm, median (IQR)	100 (46–138)	44 (22–76)	0 (0–24)	0 (0–20)	0 (0–0)	<0.001*	0.018*
Histological factors							
%Fibrosis, %	9.2 ± 4.1	7.6 ± 4.0	6.2 ± 2.8	4.8 ± 2.5	–	<0.001*	–
%Intercellular space, %	24.4 ± 8.2	22.4 ± 7.5	18.5 ± 8.4	18.2 ± 7.9	–	<0.001*	–
%Myofibrillar loss, %	25.8 ± 11.8	21.3 ± 10.6	19.5 ± 9.2	17.0 ± 8.1	–	<0.001*	–
Nuclear density, /mm <sup>2</sup>	312 ± 114	360 ± 111	410 ± 131	452 ± 163	–	<0.001*	–

\*  $p < 0.05$ ; LA volume was measured by computed tomography; ACEi, angiotensin-converting enzyme inhibitor; AF, atrial fibrillation; ARB, angiotensin II receptor blocker; BSA, body surface area; eGFR, estimated glomerular filtration rate; HFmrEF, heart failure with mid-range ejection fraction; HFpEF, heart failure with preserved ejection fraction; HFrfEF, heart failure with reduced ejection fraction; IQR, interquartile range; LA, left atrium; LS-PeAF, long-standing persistent atrial fibrillation; LV, left ventricle; LVA, low-voltage area  $< 0.5$  mV and  $\geq 3.0$  cm<sup>2</sup>; MRA, mineralocorticoid receptor antagonist; PAF, paroxysmal atrial fibrillation; PeAF, persistent atrial fibrillation; Scar, electrical scar defined as an area with  $< 0.05$  mV and  $\geq 1.0$  cm<sup>2</sup>; SCZ<sub>total</sub>, total width of slow conduction zones; V<sub>biopsy</sub>, voltage at the biopsy site; V<sub>GLA</sub>, global left atrial voltage; %Adipocyte, extent of adipocyte; %Fibrosis, extent of fibrosis; %Fractionated EGM, proportion of fractionated electrogram; %Intercellular space, extent of intercellular space; %Myofibrillar loss, severity of myofibrillar loss

**Table S2. Characteristics in patients evaluated by electron microscopy**

Variables	n = 33
Clinical parameters	
Age (range), years	69 ± 12
Female sex, n (%)	8 (24)
BSA, m <sup>2</sup>	1.71 ± 0.22
Underlying heart disease, n (%)	1 (3)
Ischemic cardiomyopathy	0 (0)
Dilated cardiomyopathy	0 (0)
Hypertrophic cardiomyopathy	1 (3)
CHA2DS2-VASc, median (IQR)	2 (1–4)
History of heart failure, n (%)	9 (27)
HF <sub>r</sub> EF	4 (12)
HF <sub>m</sub> rEF	2 (6)
HF <sub>p</sub> EF	3 (9)
Hypertension, n (%)	20 (61)
Diabetes mellitus, n (%)	3 (9)
History of stroke, n (%)	1 (3)
eGFR, mL/min/1.73 m <sup>2</sup>	61 ± 16
AF type, n (%)	
PAF	7 (21)
PeAF	10 (30)
LS-PeAF	16 (49)
Medication at baseline, n (%)	
ACEi or ARB	10 (30)
MRA	0 (0)
Diuretics (other than MRA)	0 (0)
Class I antiarrhythmic drugs	2 (6)
Beta blockers	16 (48)
Amiodarone	2 (6)
Bepridil	1 (3)
LA volume/BSA, mL/m <sup>2</sup>	100 ± 29
LA diameter, mm	42 ± 5
LV ejection fraction, %	59 ± 15
E/e'	10.0 ± 7.0
Electroanatomic characteristics	
V <sub>biopsy</sub> , mV	8.8 ± 3.1

$V_{GLA}$ , mV	$6.5 \pm 2.5$
LVA, n (%)	4 (12)
Scar, n (%)	0 (0)
%Fractionated EGM, %, median (IQR)	3.4 (1.6–5.1)
SCZ <sub>total</sub> , mm, median (IQR)	0 (0–28)
Histological parameters	
%Fibrosis, %	$7.3 \pm 3.4$
%Intercellular space, %	$19.6 \pm 7.3$
%Myofibrillar loss, %	$19.0 \pm 7.4$
Nuclear density, /mm <sup>2</sup>	$371 \pm 125$

LA volume was measured by computed tomography; ACEi, angiotensin-converting enzyme inhibitor; AF, atrial fibrillation; ARB, angiotensin II receptor blocker; BSA, body surface area; eGFR, estimated glomerular filtration rate; HF; HFmrEF, heart failure with mid-range ejection fraction; HFpEF, heart failure with preserved ejection fraction; HFrEF, heart failure with reduced ejection fraction; IQR, interquartile range; LA, left atrium; LS-PeAF, long-standing persistent AF; LV, left ventricle; LVA, presence of low-voltage area defined as  $< 0.5$  mV and  $\geq 3.0$  cm<sup>2</sup>; MRA, mineralocorticoid receptor antagonist; PAF, paroxysmal AF; PeAF, persistent AF; Scar, electrical scar defined as an area with  $< 0.05$  mV and  $\geq 1.0$  cm<sup>2</sup>; SCZ<sub>total</sub>, total width of slow conduction zones;  $V_{\text{biopsy}}$ , voltage at the biopsy site;  $V_{GLA}$ , global left atrial voltage; %Fibrosis, extent of fibrosis; %Fractionated EGM, proportion of fractionated electrograms; %Intercellular space, extent of intercellular space; %Myofibrillar loss, severity of myofibrillar loss

**Table S3. Characteristics in patients evaluated by immunohistochemical staining**

Variables	n = 60
Clinical parameters	
Age (range), years	66 ± 12
Female sex, n (%)	17 (28)
BSA, m <sup>2</sup>	1.73 ± 0.20
Underlying heart disease, n (%)	2 (3)
Ischemic cardiomyopathy	1 (1)
Dilated cardiomyopathy	1 (1)
Hypertrophic cardiomyopathy	0 (0)
CHA2DS2-VASc, median (IQR)	2 (1–4)
History of heart failure, n (%)	17 (28)
HF <sub>r</sub> EF	6 (10)
HF <sub>m</sub> rEF	3 (5)
HF <sub>p</sub> EF	8 (13)
Hypertension, n (%)	31 (52)
Diabetes mellitus, n (%)	7 (12)
History of stroke, n (%)	11 (18)
eGFR, mL/min/1.73 m <sup>2</sup>	60 ± 15
AF type, n (%)	
PAF	19 (32)
PeAF	19 (32)
LS-PeAF	22 (37)
Medication at baseline, n (%)	
ACEi or ARB	21 (35)
MRA	6 (10)
Diuretics (other than MRA)	14 (23)
Class I antiarrhythmic drugs	8 (13)
Beta blockers	35 (58)
Amiodarone	4 (7)
Bepridil	7 (12)
LA volume/BSA, mL/m <sup>2</sup>	100 ± 28
LA diameter, mm	42 ± 5
LV ejection fraction, %	60 ± 15
E/e'	10.0 ± 5.5
Electroanatomic characteristics	
V <sub>biopsy</sub> , mV	8.5 ± 3.2

$V_{GLA}$ , mV	$5.8 \pm 2.1$
LVA, n (%)	9 (15)
Scar, n (%)	1 (2)
%Fractionated EGM, %, median (IQR)	2.2 (1.3–4.4)
$SCZ_{total}$ , mm, median (IQR)	26 (0–52)
Histological parameters	
%Fibrosis, %	$8.7 \pm 4.5$
%Intercellular space, %	$19.9 \pm 9.5$
%Myofibrillar loss, %	$27.4 \pm 11.8$
Nuclear density, /mm <sup>2</sup>	$376 \pm 128$

LA volume was measured by computed tomography; ACEi, angiotensin-converting enzyme inhibitor; AF, atrial fibrillation; ARB, angiotensin II receptor blocker; BSA, body surface area; eGFR, estimated glomerular filtration rate; HFmrEF, heart failure with mid-range ejection fraction; HFpEF, heart failure with preserved ejection fraction; HFrEF, heart failure with reduced ejection fraction; IQR, interquartile range; LA, left atrium; LS-PeAF, long-standing persistent AF; LV, left ventricle; LVA, presence of low-voltage area defined as  $< 0.5$  mV and  $\geq 3.0$  cm<sup>2</sup>; MRA, mineralocorticoid receptor antagonist; PAF, paroxysmal AF; PeAF, persistent AF; Scar, electrical scar defined as an area with  $< 0.05$  mV and  $\geq 1.0$  cm<sup>2</sup>;  $SCZ_{total}$ , total width of slow conduction zones;  $V_{biopsy}$ , voltage at the biopsy site;  $V_{GLA}$ , global left atrial voltage; %Fibrosis, extent of fibrosis; %Fractionated EGM, proportion of fractionated electrograms; %Intercellular space, extent of intercellular space; %Myofibrillar loss, severity of myofibrillar loss



**Table S4. Characteristics in patients with and without a history of radiofrequency application**

Variables	All patients n = 242	Without a history of RF n = 206	With history of RF n = 36	P value
<b>Clinical parameters</b>				
Age, years	67 ± 12	67 ± 12	68 ± 11	0.663
Female sex, n (%)	73 (30)	60 (29)	13 (36)	0.433
BSA, m <sup>2</sup>	1.72 ± 0.20	1.72 ± 0.20	1.72 ± 0.19	0.973
Underlying heart disease, n (%)	16 (7)	15 (7)	1 (3)	0.479
Ischemic cardiomyopathy	3 (1)	3 (1)	0 (0)	1.000
Dilated cardiomyopathy	5 (2)	5 (2)	0 (0)	1.000
Hypertrophic cardiomyopathy	8 (3)	7 (3)	1 (3)	1.000
CHA2DS2-VASc, median (IQR)	2 (1–4)	2 (1–3)	3 (1–4)	0.577
History of heart failure, n (%)	65 (27)	56 (27)	9 (25)	0.842
HFrEF	22 (9)	21 (10)	1 (3)	0.215
HFmrEF	11 (5)	9 (4)	2 (6)	0.670
HFpEF	32 (13)	26 (13)	6 (17)	0.593
Hypertension, n (%)	137 (57)	114 (55)	23 (64)	0.368
Diabetes mellitus, n (%)	45 (19)	36 (17)	9 (25)	0.352
History of stroke, n (%)	20 (8)	17 (8)	3 (8)	1.000
eGFR, mL/min/1.73 m <sup>2</sup>	62 ± 18	63 ± 18	57 ± 16	0.039*
<b>AF type, n (%)</b>				
PAF	91 (37)	79 (38)	12 (33)	0.710
PeAF	84 (35)	75 (36)	9 (25)	0.255
LS-PeAF	67 (28)	52 (25)	15 (42)	0.067
<b>Medication at baseline, n (%)</b>				
ACEi or ARB	93 (38)	77 (37)	16 (44)	0.460
MRA	15 (6)	13 (6)	2 (6)	1.000
Diuretics (other than MRA)	33 (14)	30 (15)	3 (8)	0.433
Class I antiarrhythmic drugs	37 (15)	31 (15)	6 (17)	0.803
Beta-blockers	125 (52)	104 (50)	21 (58)	0.470
Amiodarone	23 (10)	15 (7)	8 (22)	0.010*
Bepridil	16 (7)	13 (6)	3 (8)	0.714
LA volume/BSA, mL/m <sup>2</sup>	96 ± 26	96 ± 26	93 ± 24	0.466
LA diameter, mm	41 ± 6	41 ± 6	40 ± 6	0.261
LV ejection fraction, %	62 ± 12	62 ± 12	65 ± 12	0.164
E/e'	9.7 ± 4.3	9.5 ± 4.3	10.3 ± 4.1	0.356

### Voltage parameters

$V_{\text{biopsy}}$ , mV	8.4 ± 3.1	8.5 ± 3.1	7.4 ± 2.7	0.038*
$V_{\text{GLA}}$ , mV	5.9 ± 2.3	6.1 ± 2.3	4.8 ± 1.9	<0.001*
LVA, n (%)	37 (15)	28 (14)	9 (25)	0.128
Scar, n (%)	4 (2)	1 (1)	3 (8)	0.011*
%Fractionated EGM, %, median (IQR)	2.2 (1.3–3.6)	2.2 (1.3–3.6)	1.8 (1.3–3.9)	0.756
SCZ <sub>total</sub> , mm, median (IQR)	24 (0–65)	24 (0–61)	40 (5–99)	0.071
<b>Histological parameters</b>				
%Fibrosis, %	7.0 ± 3.8	6.8 ± 3.7	8.0 ± 4.1	0.089
%Intercellular space, %	20.8 ± 8.4	20.6 ± 8.2	22.0 ± 9.5	0.396
%Myofibrillar loss, %	20.9 ± 10.4	20.7 ± 10.2	22.2 ± 12.1	0.424
Nuclear density, /mm <sup>2</sup>	384 ± 141	385 ± 143	377 ± 127	0.765
Amyloid deposition, n (%)	12 (5)	8 (4)	4 (11)	0.085

\*  $p < 0.05$ ; LA volume was measured by computed tomography; ACEi, angiotensin-converting enzyme inhibitor; AF, atrial fibrillation; ARB, angiotensin II receptor blocker; BSA, body surface area; eGFR, estimated glomerular filtration rate; HFmrEF, heart failure with mid-range ejection fraction; HFpEF, heart failure with preserved ejection fraction; HFrfEF, heart failure with reduced ejection fraction; IQR, interquartile range; LA, left atrium; LS-PeAF, long-standing persistent atrial fibrillation; LV, left ventricle; LVA, presence of low-voltage area  $< 0.5$  mV and  $\geq 3.0$  cm<sup>2</sup>; MRA, mineralocorticoid receptor antagonist; PAF, paroxysmal atrial fibrillation; PeAF, persistent atrial fibrillation; RF, radiofrequency application; Scar, electrical scar defined as an area with  $< 0.05$  mV and  $\geq 1.0$  cm<sup>2</sup>; SCZ<sub>total</sub>, total width of slow conduction zones;  $V_{\text{biopsy}}$ , voltage at the biopsy site;  $V_{\text{GLA}}$ , global left atrial voltage; %Fibrosis, extent of fibrosis; %Fractionated EGM, proportion of fractionated electrograms; %Intercellular space, extent of intercellular space; %Myofibrillar loss, severity of myofibrillar loss

**Table S5. Ultrastructural findings**

Variables	n = 33
Myofilament lysis, n (%)	30 (91)
Mitochondrial degeneration, n (%)	18 (55)
Nuclear chromatin aggregation, n (%)	11 (33)
Nuclear enlargement, n (%)	24 (73)
Autophagy, n (%)	28 (85)
Fibroblast, n (%)	33 (100)
Glycogen granules, n (%)	33 (100)
Lipid droplets, n (%)	0 (0)
ANP granules, n (%)	29 (88)
Laminarization of the capillary basement membrane, n (%)	31 (94)

ANP, atrial natriuretic peptide

**Table S6. Histological factors associated with all voltage data in the left atrium evaluated by a mixed-effects model**

Variables	Univariate		Multivariate	
	Standardized Coefficients	<i>P</i> value	Standardized Coefficients	<i>P</i> value
%Fibrosis, %	-0.600	<0.001*	-0.237	0.040*
%Intercellular space, %	-0.480	<0.001*	-0.416	<0.001*
%Myofibrillar loss, %	-0.368	<0.001*	-0.341	0.003*
%Adipocyte, %	0.118	0.216	0.093	0.335
Myocyte size, $\mu$ m	0.166	0.073	0.055	0.603
Nuclear density, /mm <sup>2</sup>	0.450	<0.001*	0.310	0.006*
Myocyte disarray, 0,1,2,3	-0.076	0.421	0.088	0.335

\*  $p < 0.05$ ; a total of 230 patients were analyzed using a mixed-effects model;  $p$  value was adjusted using the Benjamini-Hochberg method;  $V_{GLA}$ , global left atrial voltage; %Adipocyte, extent of adipocyte; %Fibrosis, extent of fibrosis; %Intercellular space, extent of intercellular space; %Myofibrillar loss, severity of myofibrillar loss.

**Table S7. Histological factors associated with each electroanatomic characteristic in male and female sex**

Variables	Standardized Coefficients							
	Multivariate							
	Male sex (n = 161)				Female sex (n = 69)			
	$V_{\text{biopsy}}$	$V_{\text{GLA}}$	%Fractionated EGM	$SCZ_{\text{total}}$	$V_{\text{biopsy}}$	$V_{\text{GLA}}$	%Fractionated EGM	$SCZ_{\text{total}}$
%Fibrosis, %	-0.180*	-0.171	0.106	0.127	-0.029	-0.145	0.123	0.212
%Intercellular space, %	-0.284‡	-0.246†	0.281†	0.255†	-0.337*	-0.321	0.208	0.387*
%Myofibrillar loss, %	-0.291†	-0.256†	0.104	0.263*	-0.362*	-0.205	0.247	0.097
%Adipocyte, %	0.123	0.068	-0.082	-0.048	0.050	0.107	-0.269	-0.001
Myocyte size, $\mu\text{m}$	0.200*	0.063	-0.055	-0.117	0.004	0.191	0.001	0.053
Nuclear density, $/\text{mm}^2$	0.272†	0.319†	-0.183	-0.171	0.234	0.296	-0.050	-0.049
Myocyte disarray, 0,1,2,3	0.090	0.056	-0.102	-0.015	-0.104	0.062	-0.098	-0.137

\*  $p < 0.05$ , †  $p < 0.01$ , ‡  $p < 0.001$ ;  $p$  value was adjusted using the Benjamini-Hochberg method in multivariate analysis;  $SCZ_{\text{total}}$ , total width of slow conduction zones;  $V_{\text{biopsy}}$ , voltage at the biopsy site;  $V_{\text{GLA}}$ , global left atrial voltage; %Adipocyte, extent of adipocyte; %Fibrosis, extent of fibrosis; %Fractionated EGM, proportion of fractionated electrogram; %Intercellular space, extent of intercellular space; %Myofibrillar loss, severity of myofibrillar loss.

**Table S8. Histological factors associated with each electroanatomic characteristic in patients with PeAF/LS-PeAF**

Variables	Standardized Coefficients							
	Univariate				Multivariate			
	$V_{\text{biopsy}}$	$V_{\text{GLA}}$	%Fractionated EGM	$SCZ_{\text{total}}$	$V_{\text{biopsy}}$	$V_{\text{GLA}}$	%Fractionated EGM	$SCZ_{\text{total}}$
%Fibrosis, %	-0.514‡	-0.434‡	0.320‡	0.401‡	-0.304†	-0.232*	0.118	0.225
%Intercellular space, %	-0.316‡	-0.313‡	0.249†	0.285‡	-0.301‡	-0.285†	0.226*	0.216†
%Myofibrillar loss, %	-0.349‡	-0.252†	0.173*	0.228†	-0.258†	-0.174	0.199	0.203
%Adipocyte, %	0.102	0.088	-0.212*	-0.088	0.075	0.060	-0.193	-0.041
Myocyte size, $\mu\text{m}$	-0.036	-0.079	0.177*	0.221†	0.063	0.093	0.049	0.143
Nuclear density, / $\text{mm}^2$	0.248†	0.309‡	-0.294‡	-0.307‡	0.142	0.243*	-0.192	-0.120
Myocyte disarray, 0,1,2,3	-0.052	-0.072	-0.002	0.103	0.105	0.066	-0.135	-0.028
Adjusted $R^2$					0.344	0.266	0.196	0.230

\*  $p < 0.05$ , †  $p < 0.01$ , ‡  $p < 0.001$ ; 144 patients were analyzed;  $p$  value was adjusted using the Benjamini-Hochberg method in multiple linear regression analysis; adjusted  $R^2$  (coefficient of determination) was calculated using all explanatory variables included in the multivariate model;  $SCZ_{\text{total}}$ , total width of slow conduction zone;  $V_{\text{biopsy}}$ , voltage at the biopsy site;  $V_{\text{GLA}}$ , global left atrial voltage; %Adipocyte, extent of adipocyte; %Fibrosis, extent of fibrosis; %Fractionated EGM, proportion of fractionated electrogram; %Intercellular space, extent of intercellular space; %Myofibrillar loss, severity of myofibrillar loss.

**Table S9. Histological factors associated with each electroanatomic characteristic in patients excluding those with radiofrequency applications before voltage mapping and those with a previous ablation**

Variables	Standardized Coefficients							
	Univariate				Multivariate			
	$V_{\text{biopsy}}$	$V_{\text{GLA}}$	%Fractionated EGM	$SCZ_{\text{total}}$	$V_{\text{biopsy}}$	$V_{\text{GLA}}$	%Fractionated EGM	$SCZ_{\text{total}}$
%Fibrosis, %	-0.514‡	-0.434‡	0.332‡	0.424‡	-0.151*	-0.190*	0.133	0.228*
%Intercellular space, %	-0.316‡	-0.313‡	0.304‡	0.364‡	-0.340‡	-0.295‡	0.272†	0.291‡
%Myofibrillar loss, %	-0.349‡	-0.252†	0.197†	0.211†	-0.303‡	-0.233†	0.219	0.219*
%Adipocyte, %	0.102	0.088	-0.099	-0.041	0.126*	0.071	-0.071	0.006
Myocyte size, $\mu\text{m}$	-0.036	-0.079	0.145*	0.230†	0.149	0.100	0.036	0.151
Nuclear density, / $\text{mm}^2$	0.248†	0.309‡	-0.262‡	-0.303‡	0.278‡	0.308‡	-0.138	-0.079
Myocyte disarray, 0,1,2,3	-0.052	-0.072	-0.010	0.048	0.038	0.088	-0.100	-0.064
Adjusted $R^2$					0.360	0.335	0.190	0.279

\*  $p < 0.05$ , †  $p < 0.01$ , ‡  $p < 0.001$ ; a total of 172 patients were analyzed;  $p$  value was adjusted using the Benjamini-Hochberg method in multiple linear regression analysis; adjusted  $R^2$  (coefficient of determination) was calculated using all explanatory variables included in the multivariate model;  $SCZ_{\text{total}}$ , total width of slow conduction zone;  $V_{\text{biopsy}}$ , voltage at the biopsy site;  $V_{\text{GLA}}$ , global left atrial voltage; %Adipocyte, extent of adipocyte; %Fibrosis, extent of fibrosis; %Fractionated EGM, proportion of fractionated electrogram; %Intercellular space, extent of intercellular space; and %Myofibrillar loss, severity of myofibrillar loss.

**Table S10. Clinical factors associated with each electroanatomic characteristic**

Variables	Standardized Coefficients							
	Univariate				Multivariate			
	$V_{\text{biopsy}}$	$V_{\text{GLA}}$	%Fractionated EGM	$SCZ_{\text{total}}$	$V_{\text{biopsy}}$	$V_{\text{GLA}}$	%Fractionated EGM	$SCZ_{\text{total}}$
Age, years	-0.406‡	-0.508‡	0.176‡	0.318‡	-0.268†	-0.314‡	0.081	0.236†
Female sex, n (%)	-0.296‡	-0.375‡	0.038	0.220‡	-0.150	-0.186*	0.050	0.235*
BSA, m <sup>2</sup>	0.361‡	0.462‡	-0.053	-0.205†	0.131	0.191*	0.053	0.089
History of HF, n (%)	-0.076	-0.166*	0.197†	0.193†	0.029	-0.007	0.132	0.051
Hypertension, n (%)	-0.044	-0.063	0.151*	0.046	0.047	0.044	0.098	-0.056
Diabetes mellitus, n (%)	0.056	0.040	-0.052	-0.073	0.060	0.037	-0.071	-0.080
PeAF/LS-PeAF, n (%)	-0.108	-0.188†	0.185†	0.212†	-0.084	-0.151*	0.048	0.109
LA volume/BSA, mL/m <sup>2</sup>	-0.277‡	-0.386‡	0.355‡	0.394‡	-0.216†	-0.266‡	0.301‡	0.327‡
LV ejection fraction, %	-0.072	-0.013	-0.061	-0.063	-0.104	-0.075	0.064	0.026
Adjusted R <sup>2</sup>					0.246	0.427	0.135	0.242

\*  $p < 0.05$ , †  $p < 0.01$ , ‡  $p < 0.001$ ; a total of 230 patients were analyzed;  $p$  value was adjusted using the Benjamini-Hochberg method in multiple linear regression analysis; adjusted R<sup>2</sup> (coefficient of determination) was calculated using all explanatory variables included in the multivariate model; LA volume was measured by computed tomography; BSA, body surface area; HF, heart failure; LA, left atrium; LS-PeAF, long-standing persistent atrial fibrillation; LV, left ventricle; PeAF, persistent atrial fibrillation;  $SCZ_{\text{total}}$ , total width of slow conduction zone;  $V_{\text{biopsy}}$ , voltage at the biopsy site;  $V_{\text{GLA}}$ , global left atrial voltage; %Fractionated EGM, proportion of fractionated electrogram



**Table S11. Histological factors associated with each electroanatomic characteristic after covariate adjustment**

Variables	Standardized Coefficients			
	$V_{\text{biopsy}}$	$V_{\text{GLA}}$	%Fractionated EGM	$\text{SCZ}_{\text{total}}$
%Fibrosis, %	-0.162*	-0.133*	0.136	0.194†
%Intercellular space, %	-0.233‡	-0.183‡	0.222‡	0.208‡
%Myofibrillar loss, %	-0.269‡	-0.160†	0.108	0.106
Nuclear density, /mm <sup>2</sup>	0.054	0.068	-0.059	-0.052
Age, years	-0.252‡	-0.267‡	0.058	0.100
BSA, m <sup>2</sup>	0.121	0.140	0.099	0.108
Female sex, n (%)	-0.135	-0.165*	0.045	0.225†
LA volume/BSA, mL/m <sup>2</sup>	-0.166†	-0.162†	0.257‡	0.265‡
PeAF/LS-PeAF, n (%)	-0.031	-0.073	-0.012	0.032

\*  $p < 0.05$ , †  $p < 0.01$ , ‡  $p < 0.001$ ; a total of 230 patients were analyzed; LA volume was measured by computed tomography; BSA, body surface area; LA, left atrium; PeAF, persistent atrial fibrillation; LS-PeAF, long-standing persistent atrial fibrillation;  $\text{SCZ}_{\text{total}}$ , total width of slow conduction zone;  $V_{\text{biopsy}}$ , voltage at the biopsy site;  $V_{\text{GLA}}$ , global left atrial voltage; %Fibrosis, extent of fibrosis; %Fractionated EGM, proportion of fractionated electrogram; %Intercellular space, extent of intercellular; %Myofibrillar loss, severity of myofibrillar loss

**Table S12. Clinical factors associated with each histological factor**

Variables	Standardized Coefficients							
	Univariate				Multivariate			
	%Fibrosis	%Intercellular space	%Myofibrillar loss	Nuclear density	%Fibrosis	%Intercellular space	%Myofibrillar loss	Nuclear density
Age, years	0.210 <sup>†</sup>	0.147*	0.117	-0.364 <sup>‡</sup>	0.097	0.129	0.017	-0.248 <sup>†</sup>
Female sex, n (%)	0.167*	0.103	0.092	-0.062	0.080	0.087	-0.014	0.005
BSA, m <sup>2</sup>	-0.226 <sup>‡</sup>	-0.117	-0.167*	0.147*	-0.139	-0.027	-0.132	0.038
History of HF, n (%)	0.137*	0.142*	0.110	-0.167*	-0.008	0.011	0.091	-0.049
Hypertension, n (%)	-0.018	-0.066	-0.058	-0.189 <sup>†</sup>	-0.072	-0.113	-0.074	-0.079
Diabetes mellitus, n (%)	0.008	-0.029	-0.041	-0.103	0.020	-0.009	-0.036	-0.081
PeAF/LS-PeAF, n (%)	0.212 <sup>†</sup>	0.217 <sup>†</sup>	0.049	-0.244 <sup>‡</sup>	0.181*	0.214*	0.019	-0.116
LA volume/BSA, mL/m <sup>2</sup>	0.297 <sup>‡</sup>	0.151*	0.182 <sup>†</sup>	-0.408 <sup>‡</sup>	0.194*	0.027	0.176	-0.287 <sup>‡</sup>
LV ejection fraction, %	-0.104	-0.147*	0.044	0.054	-0.042	-0.117	0.137	-0.021
Adjusted R <sup>2</sup>					0.132	0.071	0.040	0.241

\*  $p < 0.05$ , <sup>†</sup>  $p < 0.01$ , <sup>‡</sup>  $p < 0.001$ ; a total of 230 patients were analyzed;  $p$  value was adjusted using the Benjamini-Hochberg method in multiple linear regression analysis; adjusted R<sup>2</sup> (coefficient of determination) was calculated using all explanatory variables included in the multivariate model; LA volume was measured by computed tomography; BSA, body surface area; HF, heart failure; LA, left atrium; LS-PeAF, long-standing persistent atrial fibrillation; LV, left ventricle; PeAF, persistent atrial fibrillation; %Fibrosis, extent of fibrosis; %Intercellular space, extent of intercellular space; %Myofibrillar loss, severity of myofibrillar loss.

**Table S13. Histological factors associated with V<sub>GLA</sub> in Q1 or Q2–Q4**

Variables	Standardized Coefficients		
	Multivariate		
	All patients n = 230	Q1, < 4.2 mV n = 57	Q2Q3Q4, ≥ 4.3 mV n = 173
%Fibrosis, %	0.198 <sup>†</sup>	0.382 <sup>*</sup>	0.182 <sup>*</sup>
%Intercellular space, %	0.251 <sup>‡</sup>	0.092	0.202 <sup>†</sup>
%Myofibrillar loss, %	0.243 <sup>‡</sup>	0.098	0.177 <sup>*</sup>
Nuclear density, /mm <sup>2</sup>	0.240 <sup>‡</sup>	0.032	0.193 <sup>*</sup>

\*  $p < 0.05$ , †  $p < 0.01$ , ‡  $p < 0.001$ ; %Fibrosis, extent of fibrosis; %Intercellular space, extent of intercellular space; %Myofibrillar loss, severity of myofibrillar loss

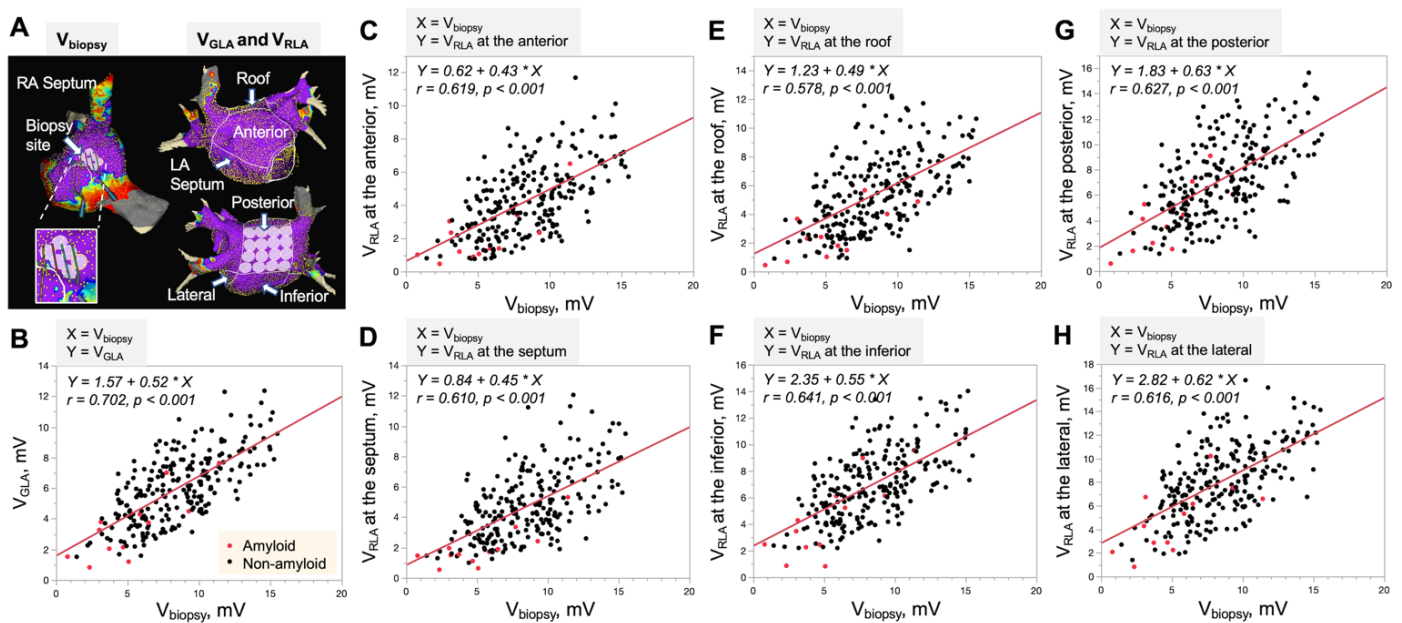
**Table S14. Patient characteristics of autopsy cases**

Case	Age (years)	Sex	BSA	Cause of death	Endocardium, $\mu\text{m}$					
					A	S	R	I	P	L
1	87	Male	1.27	Pneumonia	576	813	447	797	928	663
2	73	Male	1.62	Hepatocellular carcinoma	691	697	519	584	548	502
3	69	Female	1.19	Calciphylaxis	694	855	302	845	1240	411
4	77	Male	1.57	Interstitial pneumonia	572	931	597	505	387	217
5	84	Female	1.66	Sepsis	450	760	375	495	465	132
6	70	Female	1.17	Pneumocystis pneumonia	502	686	677	632	652	512
7	66	Male	1.76	Fulminant myocarditis	269	1113	619	765	362	512
8	83	Male	1.33	Pneumonia	771	964	678	814	424	538
Mean	76	–	1.45	–	566	852	526	680	626	436

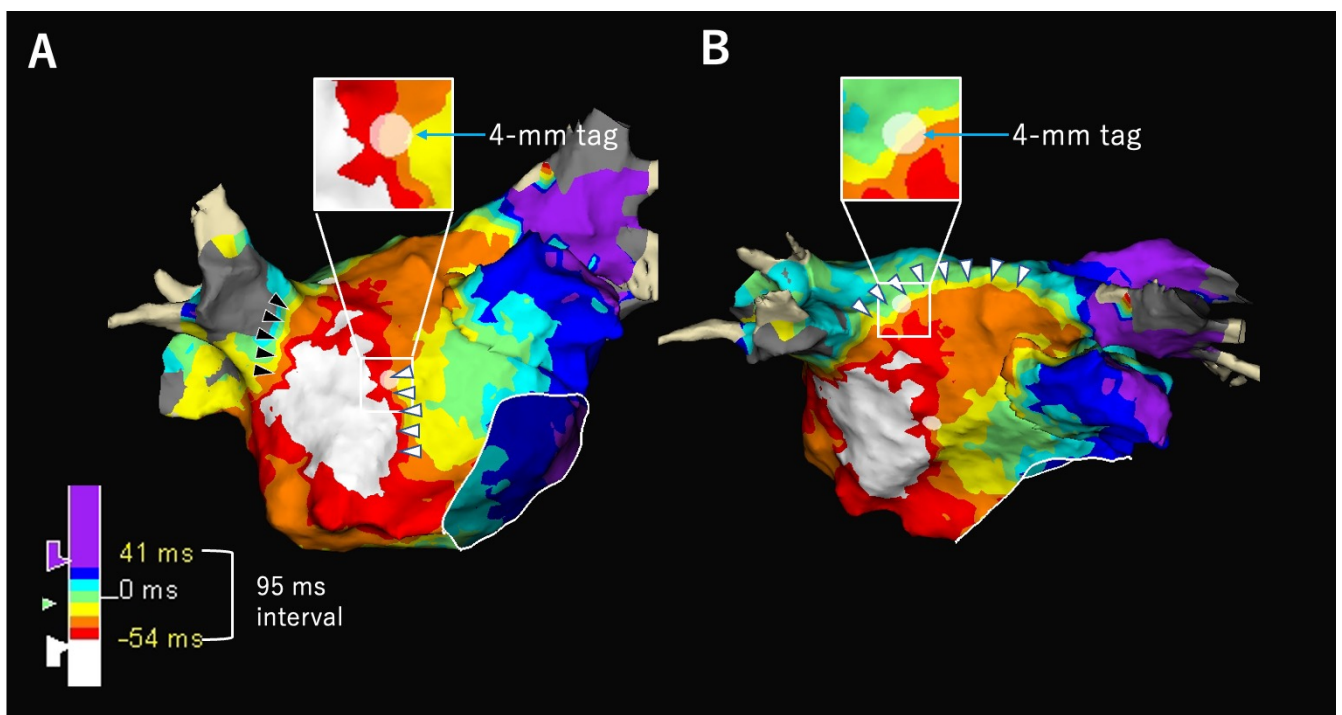
A: left atrial anterior region, AF: atrial fibrillation, BSA: body surface area, I: left atrial inferior region, L: left atrial lateral region, P: left atrial posterior region, R: left atrial roof region, S: right atrial septum.

**Supplementary Figure S1.** Example of voltage analysis. The biopsy site was subdivided into six 0.25 cm<sup>2</sup> areas on the RA voltage map, and the  $V_{\text{biopsy}}$  was measured as the mean of the six highest peak-to-peak bipolar voltages in each 0.25 cm<sup>2</sup> area. LA, excluding the LA ridge, PV, LAA, and mitral annular region, was subdivided into areas of 1.0 cm<sup>2</sup>, and global LA voltage ( $V_{\text{GLA}}$ ) was measured as the mean highest peak-to-peak bipolar voltage in each 1.0 cm<sup>2</sup> area in the entire LA. LA was subdivided into anterior, septum, roof, inferior, posterior, and lateral regions.  $V_{\text{RLA}}$  corresponding to the six anatomical regions was also evaluated as the mean of the highest voltage in each 1 cm<sup>2</sup> area (A). The associations between  $V_{\text{biopsy}}$  and  $V_{\text{GLA}}$  (B), and between  $V_{\text{biopsy}}$  and  $V_{\text{RLA}}$  in the anterior, septum, roof, inferior, posterior, and lateral regions are shown (C–H). Red dot indicates a patient with amyloid deposition.

LA, left atrium; LAA, left atrial appendage; PV, pulmonary vein;  $V_{\text{biopsy}}$ , voltage at the biopsy site;  $V_{\text{GLA}}$ , global left atrial voltage;  $V_{\text{RLA}}$ , regional left atrial voltage

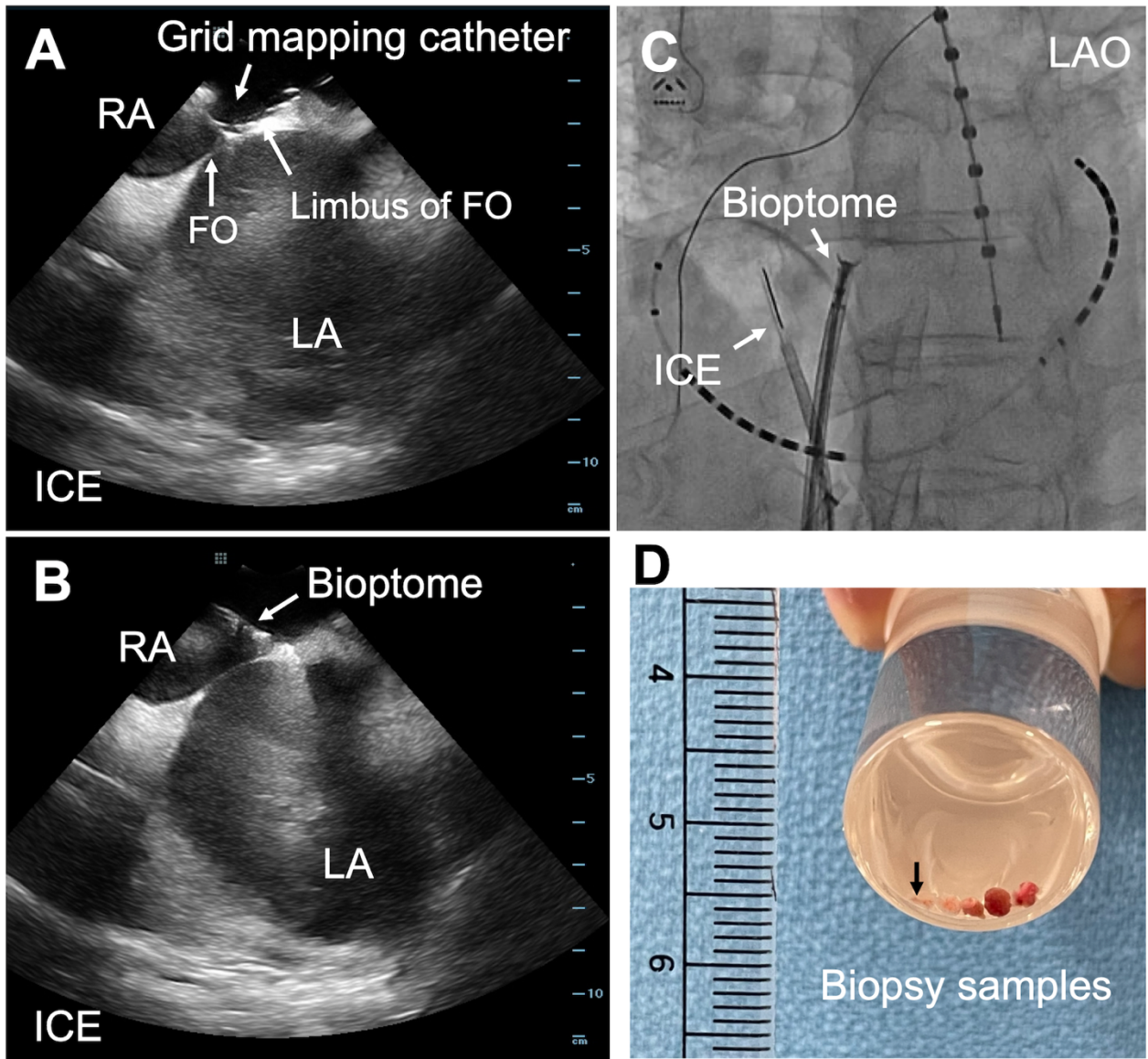


**Supplementary Figure S2.** Analysis of local slow conduction zones (SCZs). Examples of SCZs at the anterior wall (A) and roof (B) were shown (white arrow heads). The interval between color bar was set to 95 ms, which was divided into seven segments with eight colors from white to purple. Then, the conduction velocity across the 4-mm tag is calculated as 29 cm/s (<30cm/s). When one or more isochrone was identified in the 4-mm tag with a width of 20 mm or more, we counted it as a SCZ and measured the width of the SCZ and then calculated the total width of SCZs (SCZ<sub>total</sub>) in each patient. A tag with a diameter of 4 mm was shown in the box as a reference. The width of SCZs at the anterior wall and the roof were 24 mm and 34 mm, respectively. The SCZ<sub>total</sub> in this case was calculated as 58 mm. SCZs along the ostium of the pulmonary vein (PV) or inside PV were excluded from the analysis. The black arrow heads show a SCZ along the right superior PV ostium.

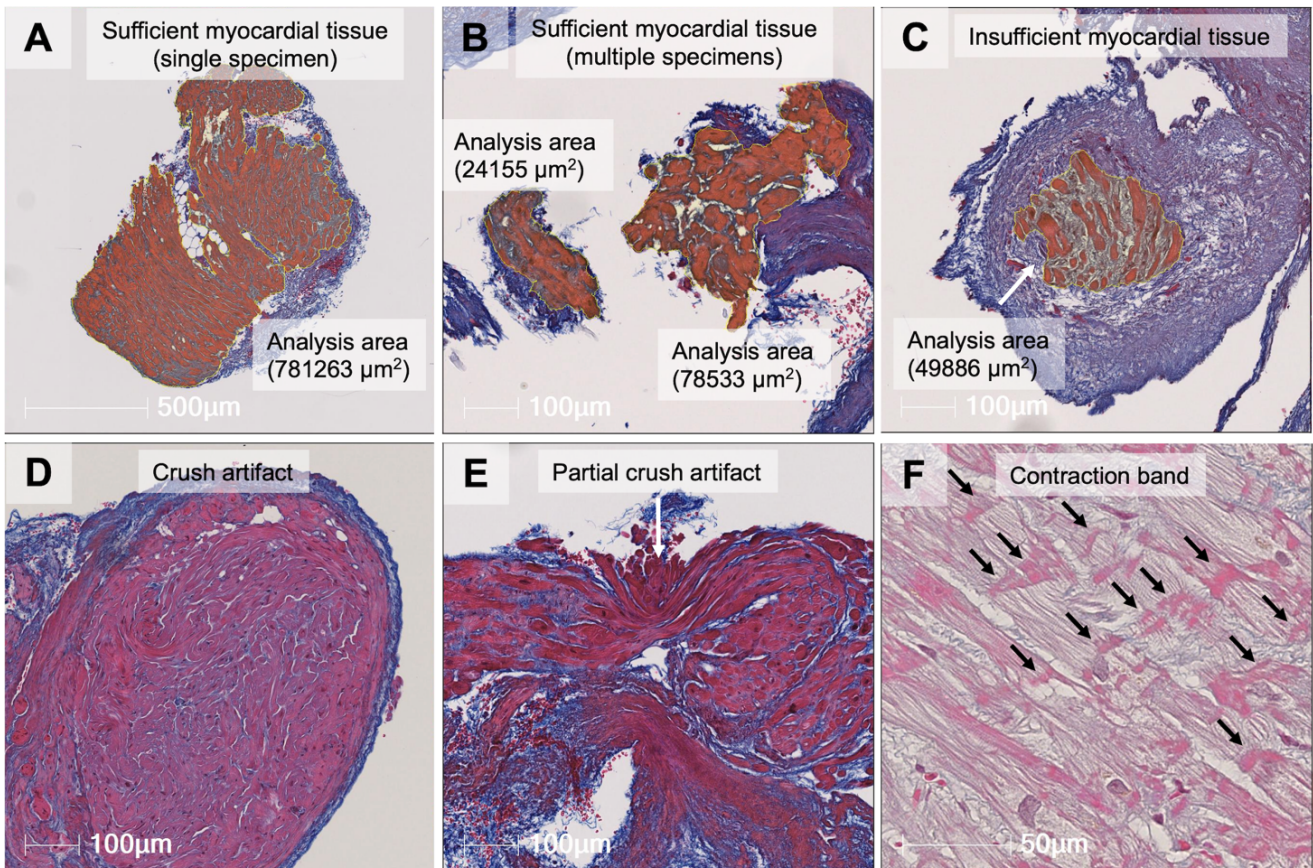


**Supplementary Figure S3.** Biopsy samples were obtained from the posterior side of the limbus of the FO under ICE and fluoroscopy guidance (A, B, C). 1 to 3 mm biopsy samples are shown (D). The sample indicated by the arrow apparently has only endocardium, which was obtained by the first biopsy. Myocardial tissues were obtained by the subsequent biopsies at the same location.

FO, fossa ovalis; ICE, intracardiac echocardiography; LA, left atrium; LAA, left atrial appendage; LAO, left anterior oblique; RA, right atrium



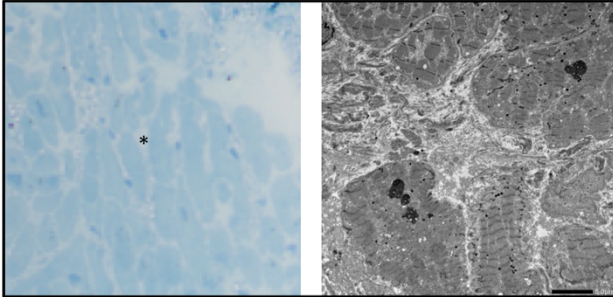
**Supplementary Figure S4.** Biopsy samples excluded from the analyses. Sufficient myocardial tissue of the biopsy samples for histological examination was defined as a total analysis area of  $\geq 100,000 \mu\text{m}^2$ . Examples of biopsy samples with sufficient myocardial tissue in a single specimen (A) or multiple specimens (B), and an example of insufficient myocardial tissue with a total analysis area of  $< 100,000 \mu\text{m}^2$  are shown (C). Examples of myocardial tissue with crush artifact in the entire specimen (D), a partial crush artifact (E), or contraction band (F) are shown, all of which were excluded from the analysis.



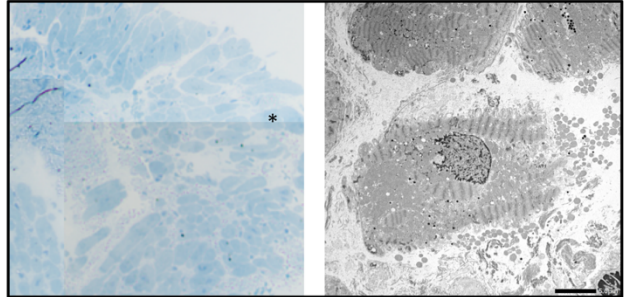


**Supplementary Figure S5.** Tissue preparation and evaluation by transmission electron microscopy. Five randomly designated parenchymal and five interstitial sites were observed by electron microscopy. Electron microscopic images of two interstitial regions (interstitium 1 and 2) and two parenchymal regions (myocardium 1 and 2) designated on the ultrathin sections stained with uranyl acetate in a patient are shown.

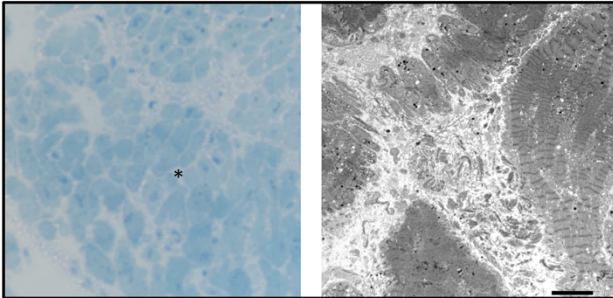
Interstitium 1



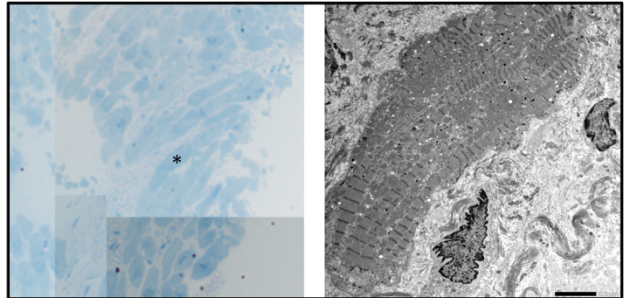
Myocardium 1



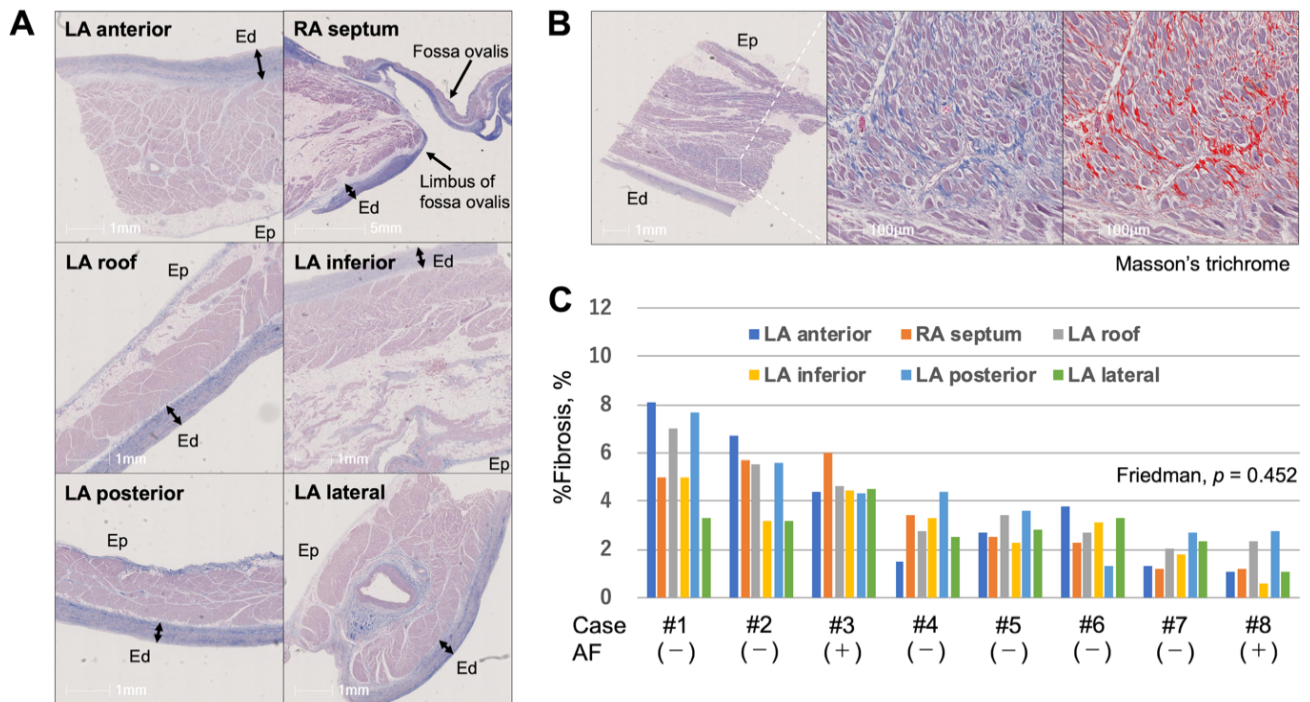
Interstitium 2



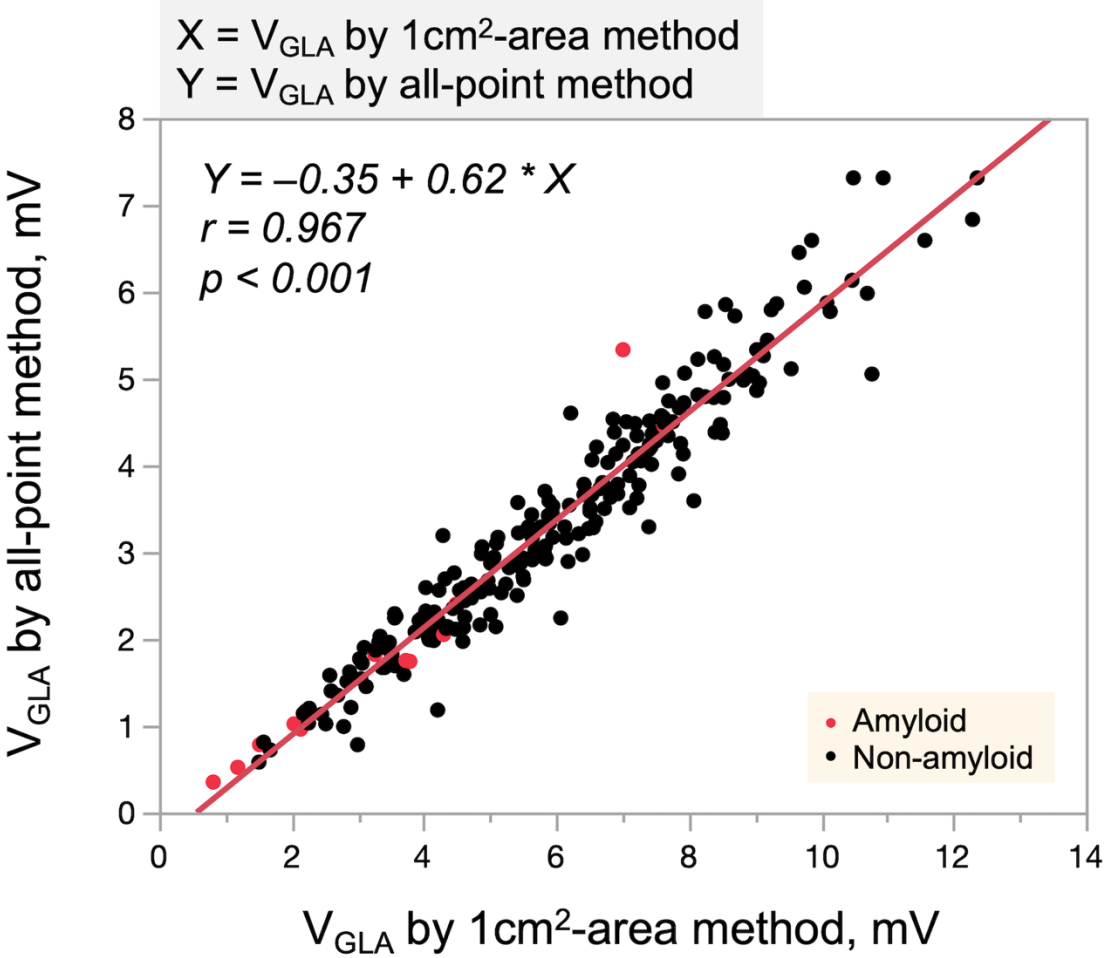
Myocardium 2



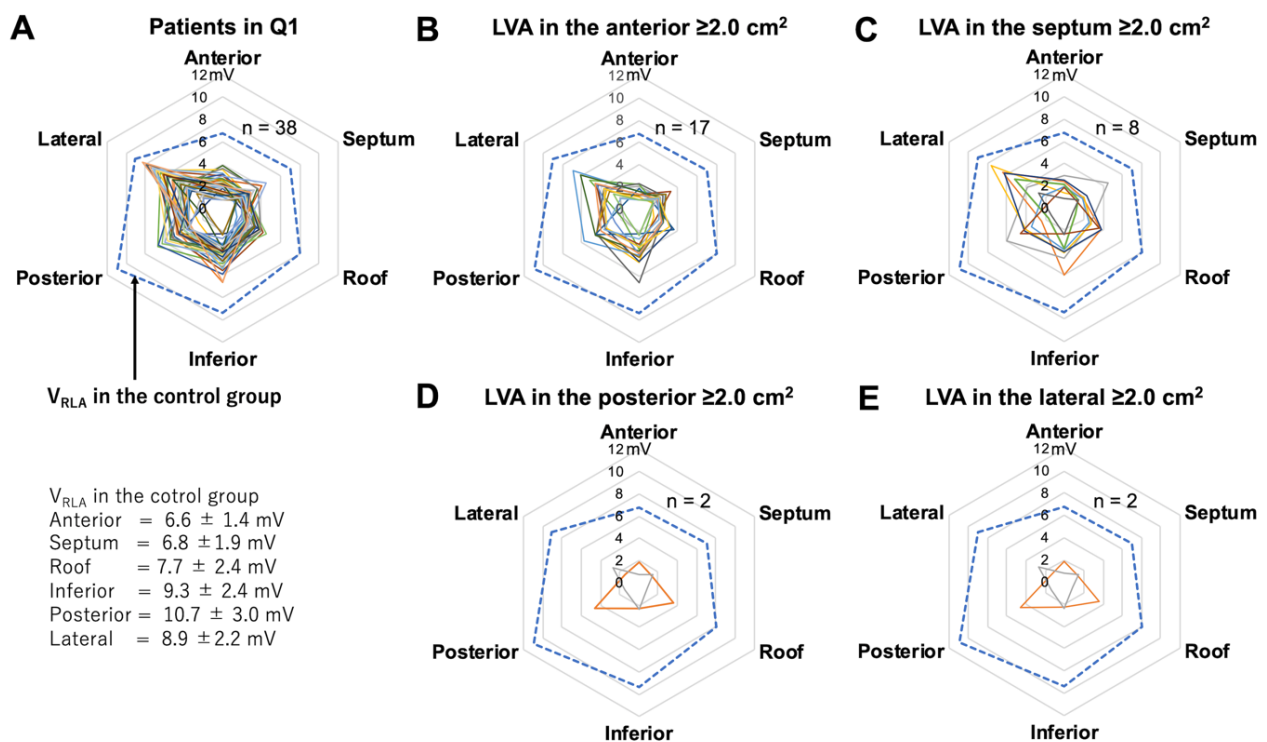
**Supplementary Figure S6.** Analysis of autopsy samples. To measure %Fibrosis, five analysis areas of approximately 1.0 mm<sup>2</sup> were randomly selected on the endocardial side in the RA septum and each LA region including the anterior, roof, inferior, posterior, and lateral regions, and the mean value of %Fibrosis was calculated (A). This example corresponds to Case 3 (B). There was no significant difference in %Fibrosis between the regions (C). Ed, endocardium; Ep, epicardium; FO, fossa ovalis; LA, left atrium; RA, right atrium; %Fibrosis, extent of fibrosis



**Supplementary Figure S7.** The association between  $V_{GLA}$  using the 1 cm<sup>2</sup>-area method and the all-annotated-point method is shown. Red dot indicates a patient with amyloid deposition.  $V_{GLA}$ , global left atrial voltage

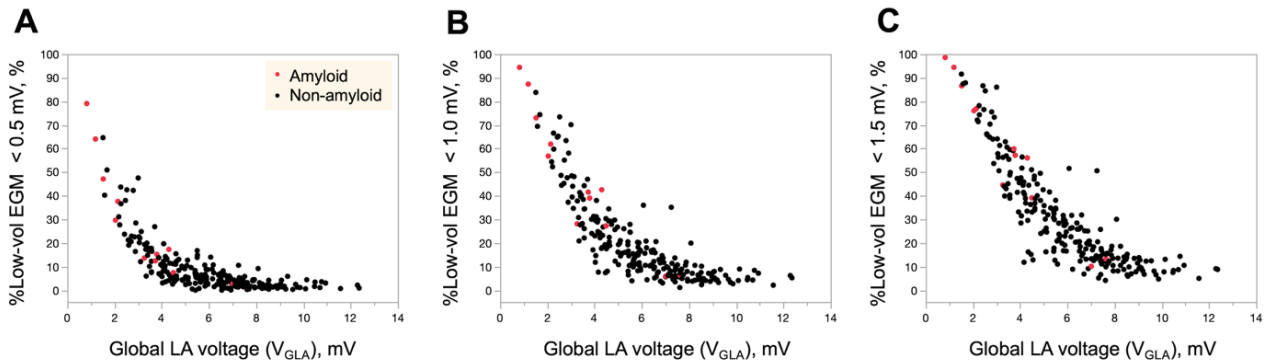


**Supplementary Figure S8.** The radar charts show comparison of regional left atrial (LA) voltage ( $V_{RLA}$ ) according to the six anatomical LA regions (anterior, septum, roof, inferior, posterior and lateral wall) in patients categorized into the Q1 of  $V_{GLA}$  ( $n=38$ ) (A), those with low-voltage area (LVA) in the anterior wall ( $n=17$ ) (B), LVA in the septum ( $n=8$ ) (C), LVA in the posterior ( $n=2$ ) (D), and LVA in the lateral wall ( $n=2$ ) (E). Each line indicates  $V_{RLA}$  of each patient. The mean  $V_{RLA}$  of the six anatomical regions in the control group (the values were shown in the figure) was also shown as a reference (outermost blue dashed line). LVA was defined as an area with  $<0.5\text{mV}$  and  $\geq 2.0\text{ cm}^2$ . All patients classified into Q1 had lower  $V_{RLA}$  in all LA regions than that of the control group. All patients with LVA identified in any LA region had lower  $V_{RLA}$  in all LA regions than that of the control group. Patients with history of pulmonary vein isolation (PVI) were excluded from this analysis. Patients who underwent voltage mapping after PVI were also excluded.



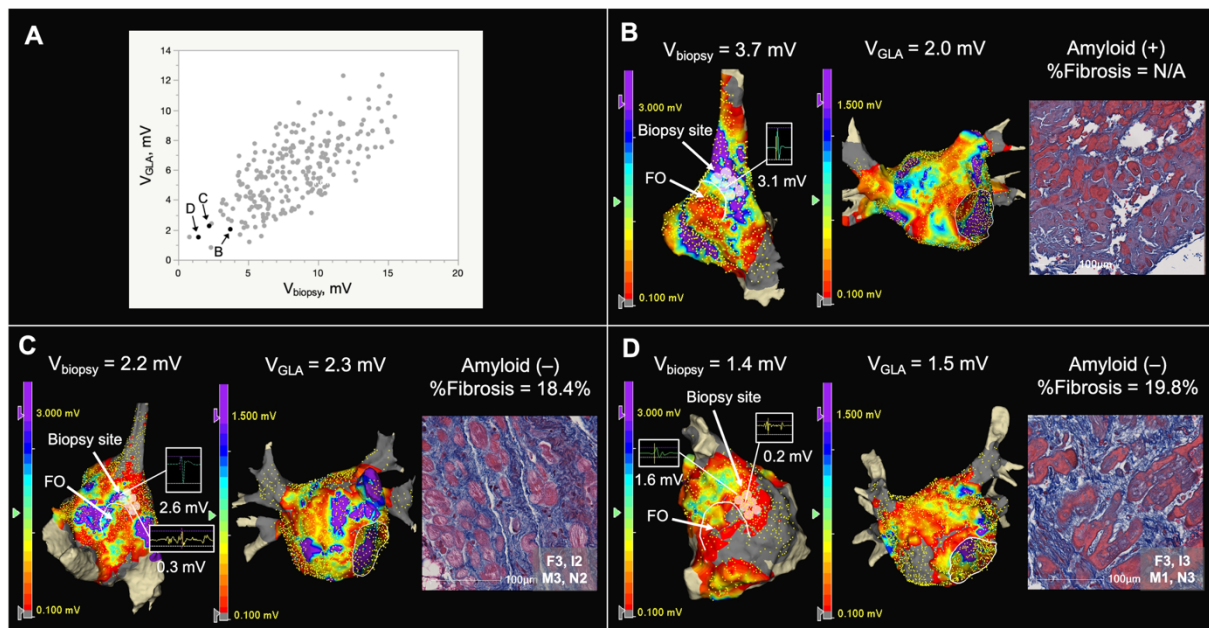
**Supplementary Figure S9.** The association between  $V_{GLA}$  using the 1 cm<sup>2</sup>-area method and the proportion of low-voltage electrograms (%Low-vol EGM) defined as <0.5 mV, <1.0 mV, and <1.5 mV. %Low-vol EGM defined as <0.5 mV, <1.0 mV, and <1.5mV increased as  $V_{GLA}$  decreased below 4 mV, 6 mV, and 8 mV, respectively, showing that the increase of low-voltage electrograms in the LA is closely associated with reduction in  $V_{GLA}$ . Red dot indicates a patient with amyloid deposition.

$V_{GLA}$ , global left atrial voltage

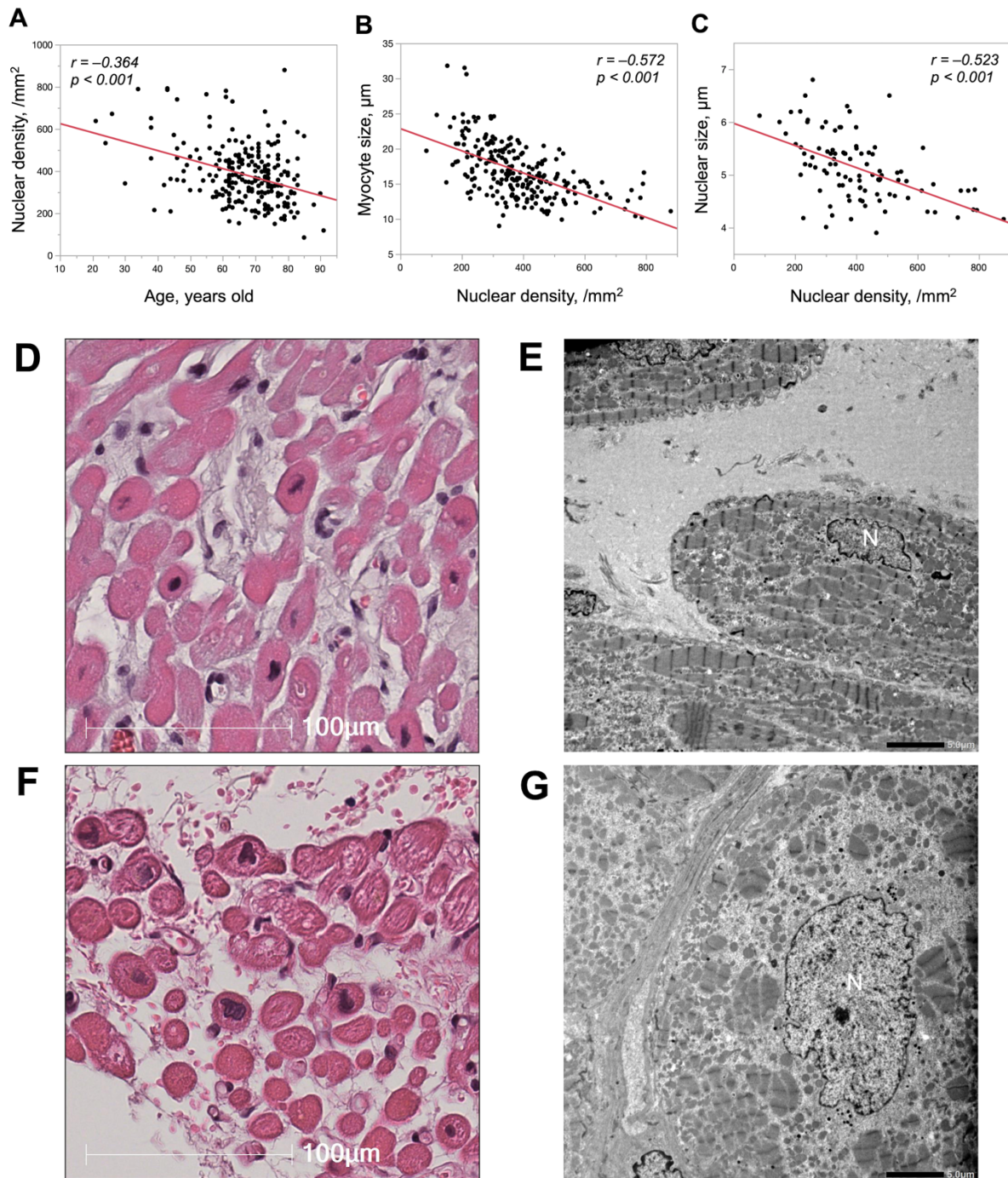


**Supplementary Figure S10.** Scatter plots between  $V_{\text{biopsy}}$  and  $V_{\text{GLA}}$ , in which case B, C, and D are shown (A). Examples of voltage maps of the RA septum and the whole LA, and histological findings at the biopsy site in three patients with the lowest voltage. Histology shows amyloid deposition (B), a high degree of fibrosis (C, D) (Masson's trichrome staining). In case B, amyloid deposition was confirmed by Congo red staining and apple-green birefringence under a polarizing microscope (data not shown).

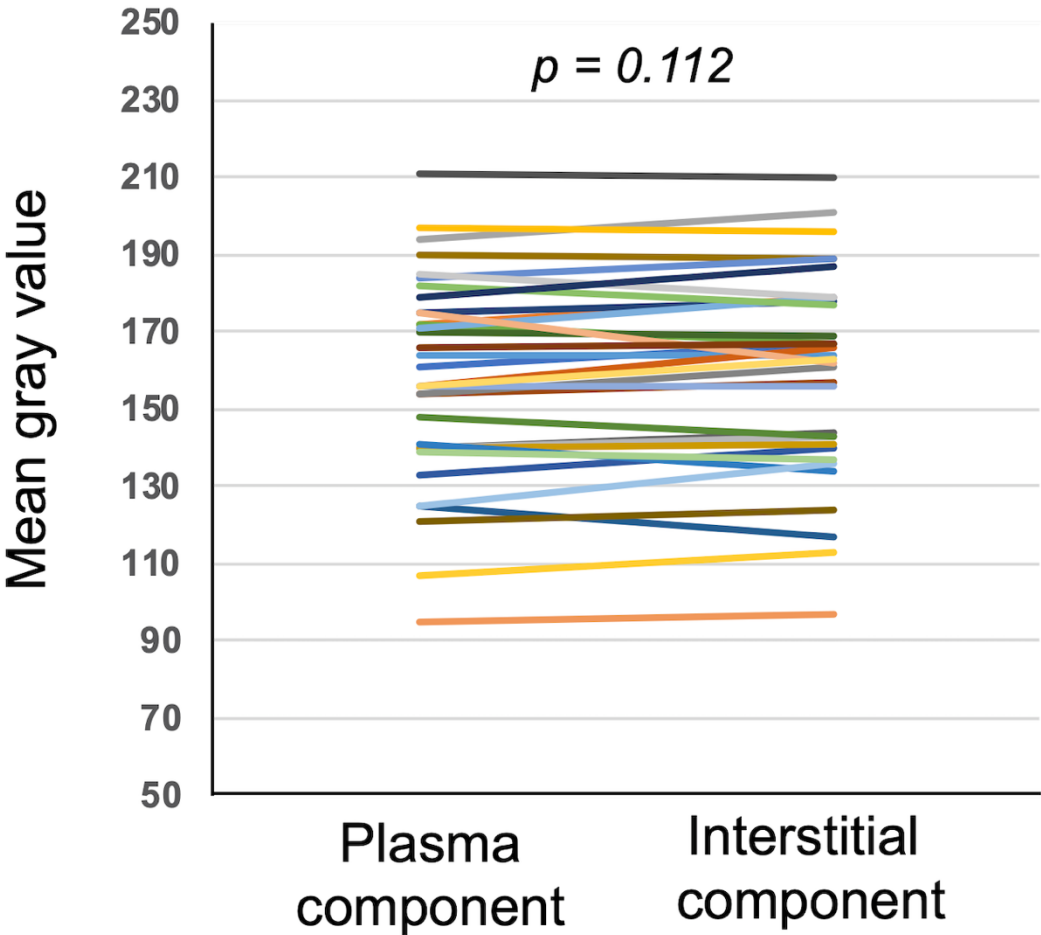
FO, fossa ovalis; LA, left atrium; RA, right atrium;  $V_{\text{biopsy}}$ , voltage at the biopsy site;  $V_{\text{GLA}}$ , global left atrial voltage; %Fibrosis, extent of fibrosis.



**Supplementary Figure S11.** Associations between nuclear density and age (A), myocyte size (B), and nuclear size (C) are shown. Examples of normal and enlarged nuclei on light microscopy and electron microscopy were shown in Figure D and E, and Figure F and G, respectively. Scale bars = 100  $\mu\text{m}$  in (D and F) and 5  $\mu\text{m}$  in (E and G).

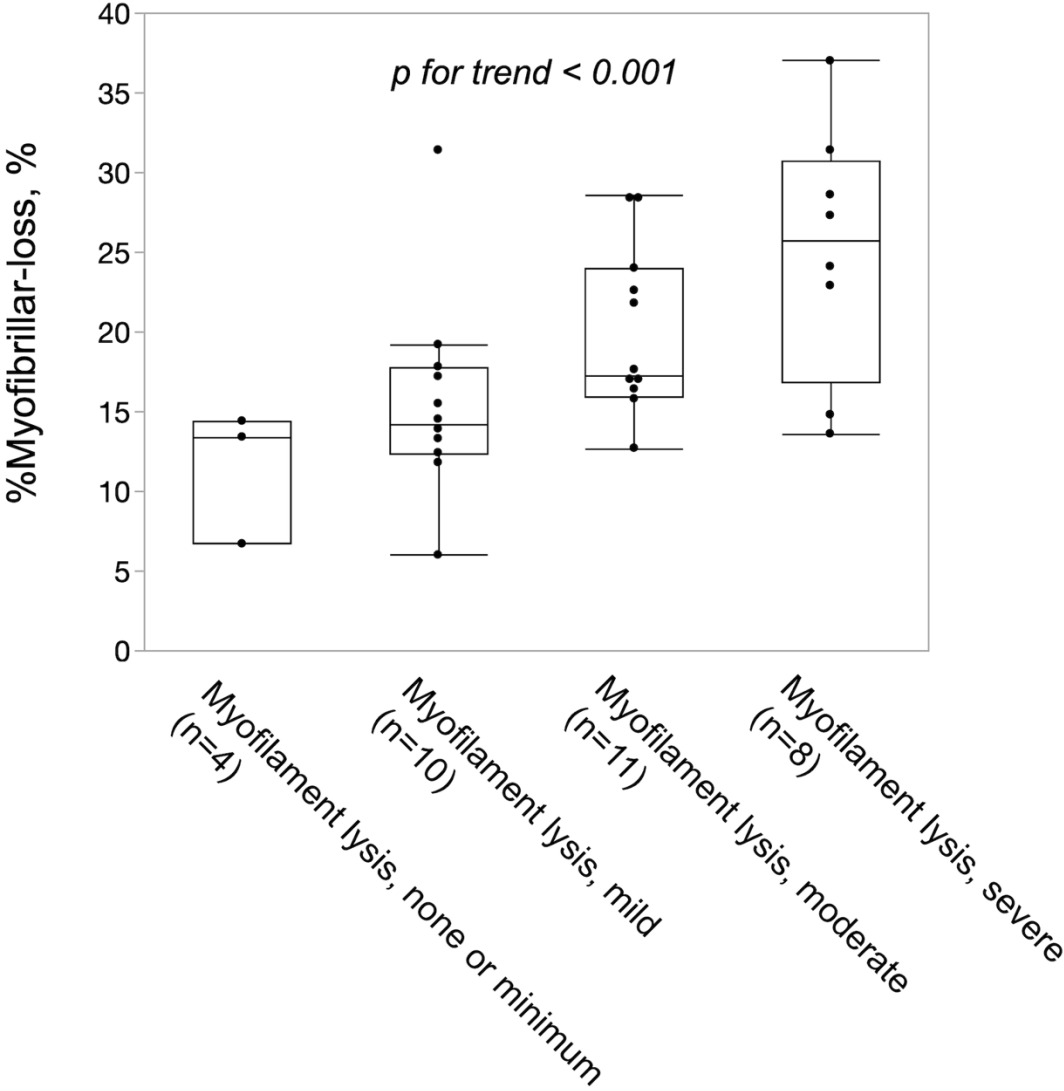


**Supplementary Figure S12.** A comparison of the mean gray value (electron density) between the area without obvious structures in the increased intercellular spacings and the plasma components in the capillaries. ImageJ was used for the measurement of the mean gray value.



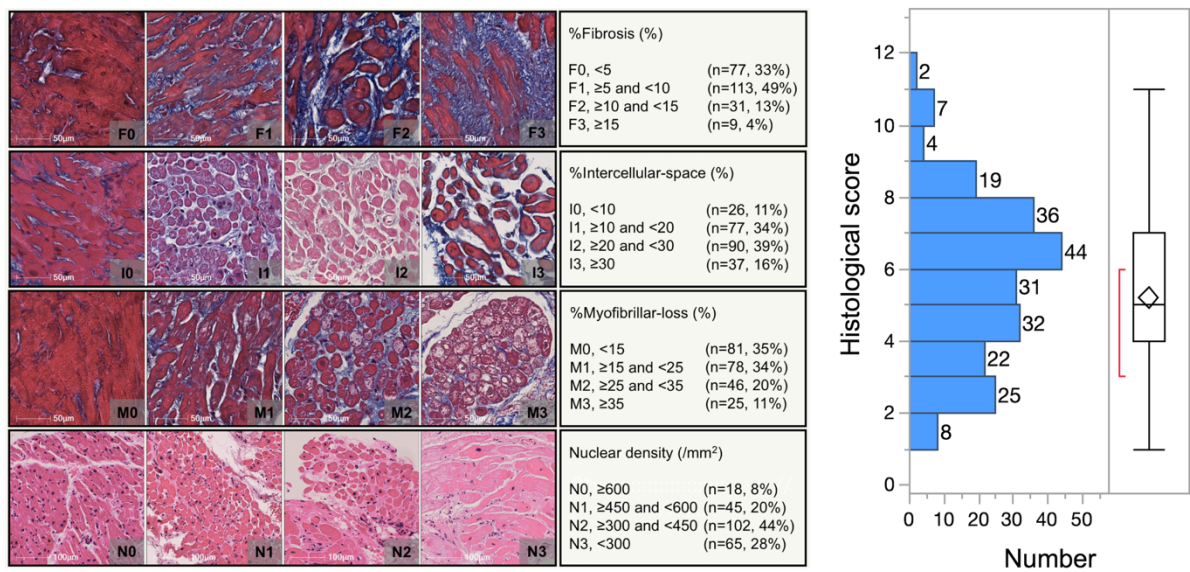


**Supplementary Figure S13.** A comparison between the severity of myofilament lysis on electron microscopy and %Myofibrillar loss on light microscopy.

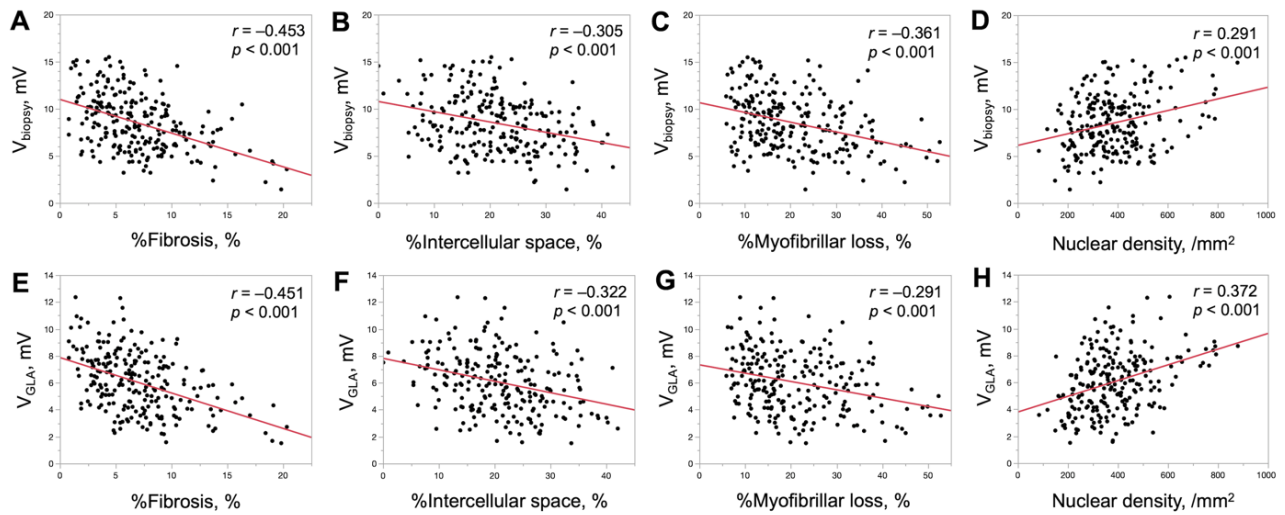


**Supplementary Figure S14.** Tentative criteria for semi-quantification of %Fibrosis, %Intercellular space, %Myofibrillar loss, and myocardial nuclear density are shown in the figure with histological images. Minimum was scored as 0, mild as 1, moderate as 2, and severe as 3, and the total of the four scores was calculated as the histological score. The distribution of histological scores is also shown. All patients had a histological score of 1 or higher.

%Fibrosis, extent of fibrosis; %Intercellular space, extent of intercellular space; %Myofibrillar loss, severity of myofibrillar loss

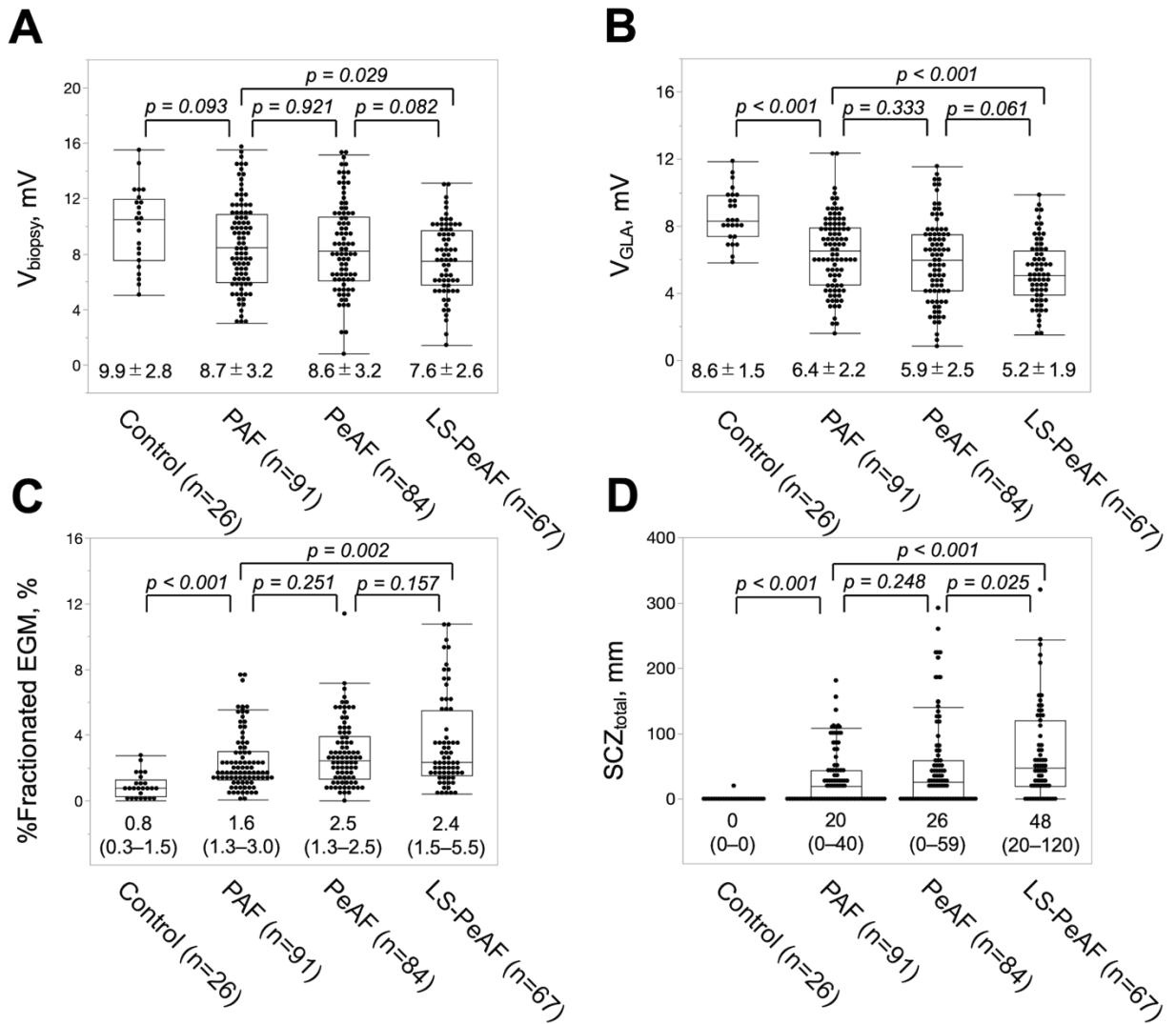


**Supplementary Figure S15.** Scatter plots of the histological factors and voltage. The association between %Fibrosis, %Intercellular space, %Myofibrillar loss, nuclear density, and  $V_{\text{biopsy}}$  (**A, B, C, and D**, respectively), and  $V_{\text{GLA}}$  (**E, F, G, and H**, respectively) are shown.  $V_{\text{biopsy}}$ , voltage at the biopsy site;  $V_{\text{GLA}}$ , global left atrial voltage; %Fibrosis, extent of fibrosis; %Intercellular space, extent of intercellular space; %Myofibrillar loss, severity of myofibrillar loss

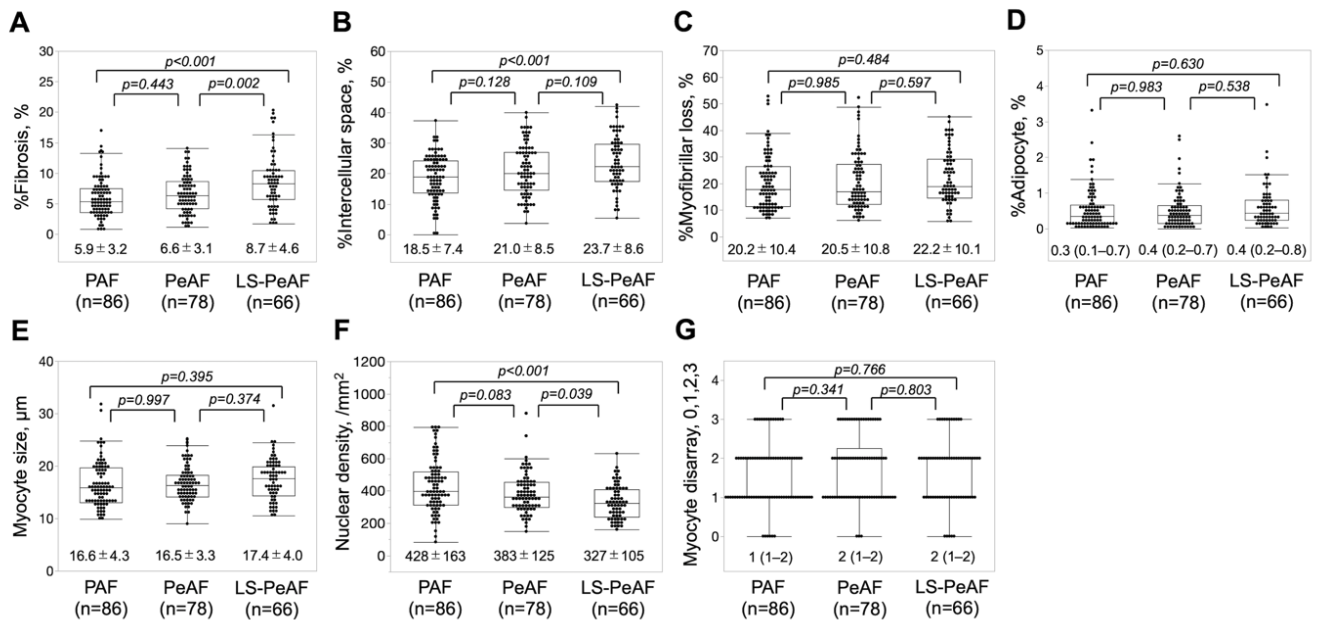


**Supplementary Figure S16.** Relationship between atrial fibrillation (AF) type and each electroanatomic characteristic. Comparisons were also performed between the PAF group and the control group.

LS-PeAF, long-standing persistent AF; PAF, paroxysmal AF; PeAF, persistent AF; SCZ<sub>total</sub>, total width of the slow conduction zones; V<sub>biopsy</sub>, voltage at the biopsy site; V<sub>GLA</sub>, global left atrial voltage; %Fractionated EGM, proportion of the fractionated electrograms

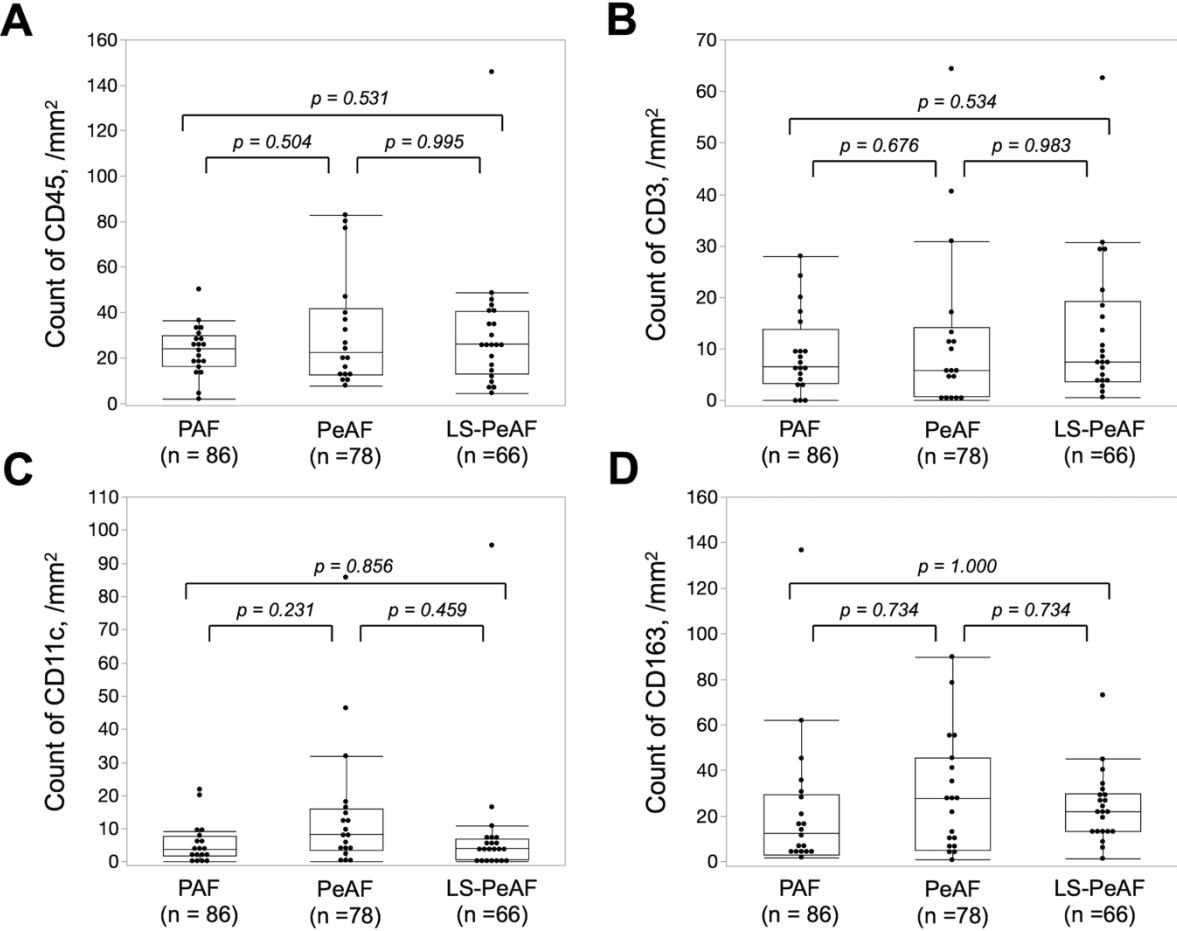


**Supplementary Figure S17.** Relationship between atrial fibrillation (AF) type and each histological factor. Patients in the amyloid group (n=12) were excluded from the analyses. LS-PeAF, long-standing persistent AF; PAF, paroxysmal AF; PeAF, persistent AF; %Fibrosis, extent of fibrosis; %Intercellular space, extent of intercellular space; %Myofibrillar loss, severity of myofibrillar loss



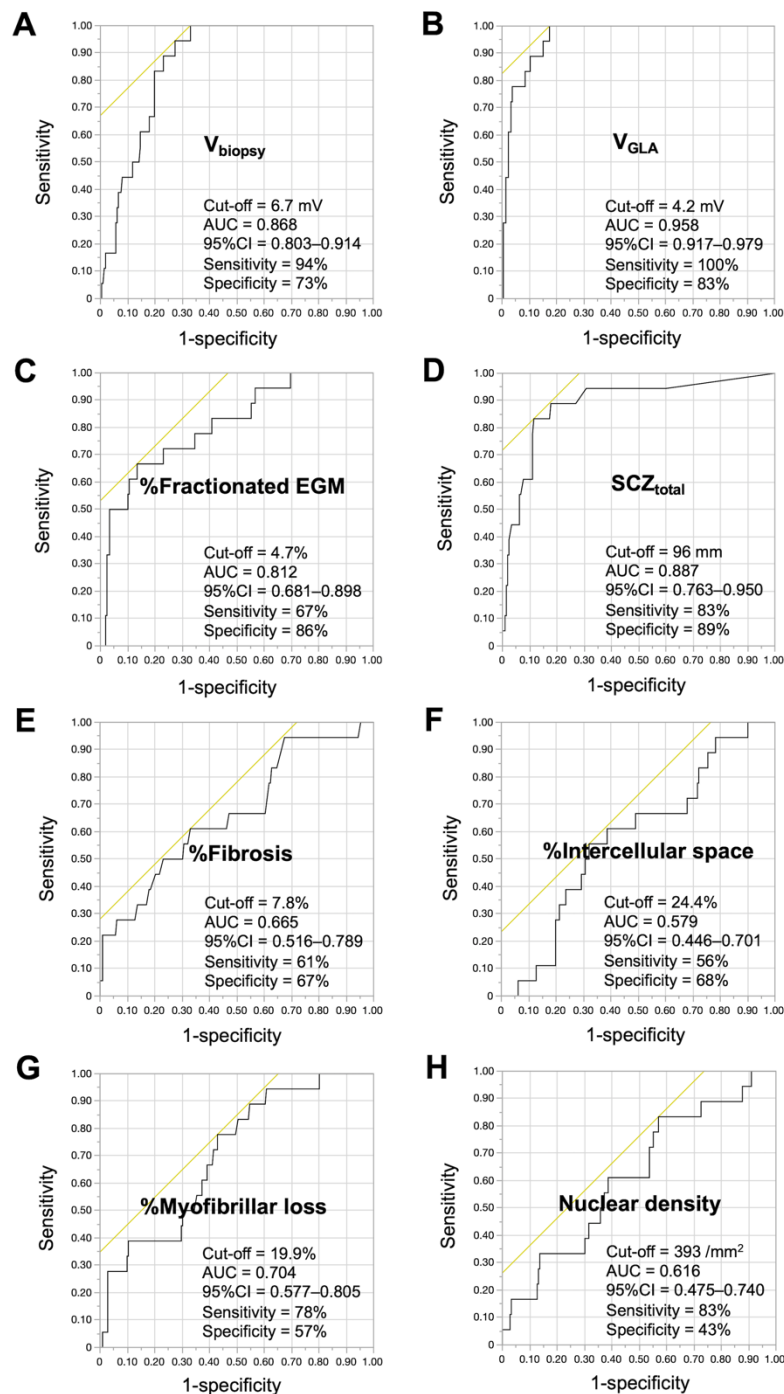
**Supplementary Figure S18.** Relationship between atrial fibrillation (AF) type and inflammatory cell infiltration.

LS-PeAF, long-standing persistent AF; PAF, paroxysmal AF; PeAF, persistent AF



**Supplementary Figure S19.** Receiver operation curves (ROC) for each electroanatomic characteristic and histological factor for the inducibility of left atrial macroreentrant tachycardia (LAMRT) after pulmonary vein isolation.

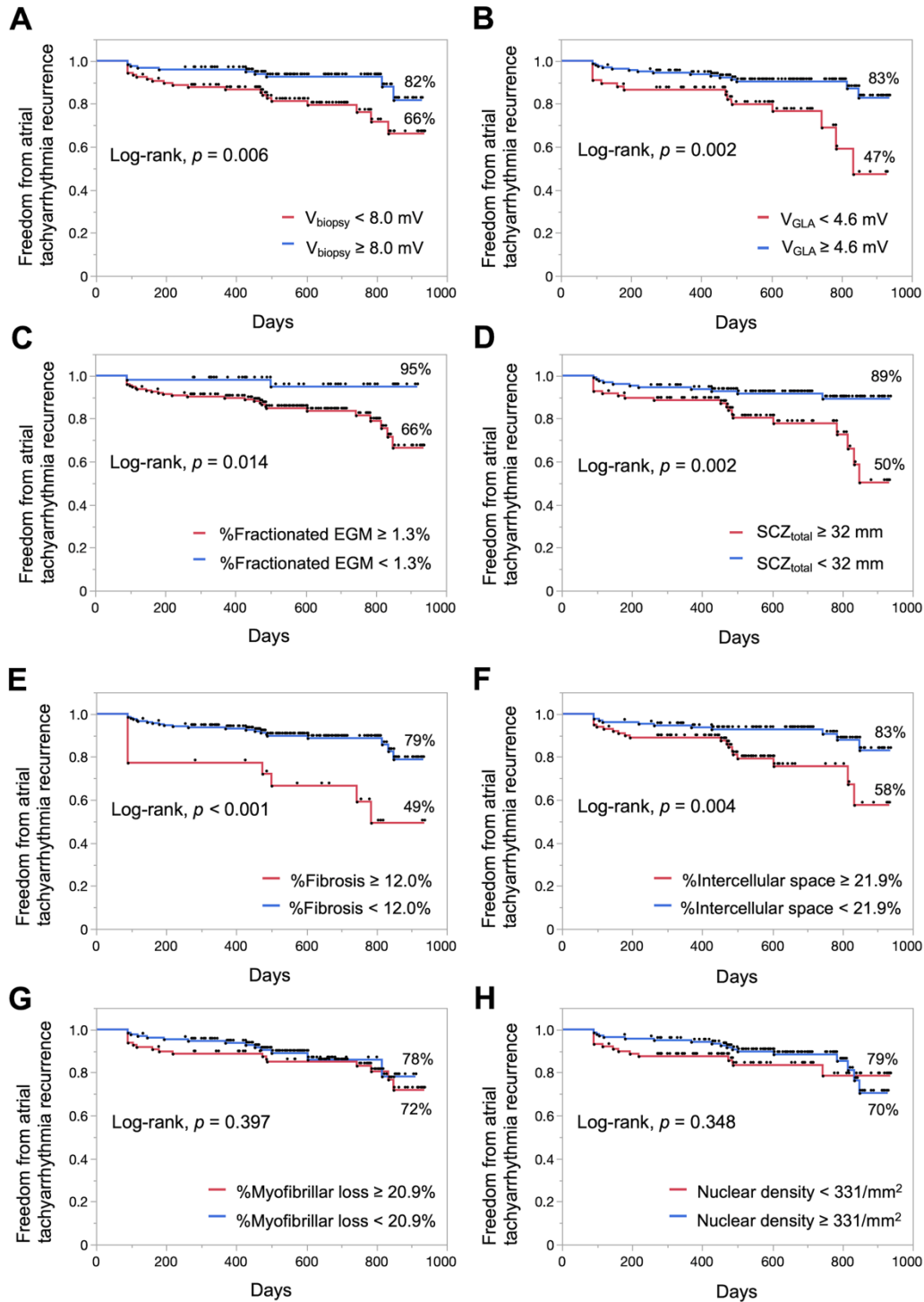
AUC, area under the ROC curve; CI, confidence interval; LS-PeAF, long-standing persistent atrial fibrillation; PAF, paroxysmal atrial fibrillation; PeAF, persistent atrial fibrillation; SCZ<sub>total</sub>, total width of the slow conduction zones; V<sub>biopsy</sub>, voltage at the biopsy site; V<sub>GLA</sub>, global left atrial voltage; %Fibrosis, extent of fibrosis; %Fractionated EGM, proportion of the fractionated electrograms; %Intercellular space, extent of intercellular space; %Myofibrillar loss, severity of myofibrillar loss



**Supplementary Figure S20.** Atrial tachyarrhythmia recurrence stratified by electroanatomic characteristics and histological factors.

SCZ<sub>total</sub>, total width of the slow conduction zones; V<sub>biopsy</sub>, voltage at the biopsy site; V<sub>GLA</sub>, global left atrial voltage

%Fibrosis, extent of fibrosis; %Fractionated EGM, proportion of the fractionated electrograms; %Intercellular space, extent of intercellular space; %Myofibrillar loss, severity of myofibrillar loss





## References

1. Calkins H, Hindricks G, Cappato R, Kim YH, Saad EB, Aguinaga L, et al. 2017 HRS/EHRA/ECAS/APHS/SOLAECE expert consensus statement on catheter and surgical ablation of atrial fibrillation: Executive summary. *J Arrhythm*. 2017;33:369–409.
2. Yamaguchi T, Otsubo T, Takahashi Y, Nakashima K, Fukui A, Hirota K, et al. Atrial structural remodeling in patients with atrial fibrillation is a diffuse fibrotic process: evidence from high-density voltage mapping and atrial biopsy. *J Am Heart Assoc*. 2022;11:e024521.
3. Deno DC, Bhaskaran A, Morgan DJ, Goksu F, Batman K, Olson GK, et al. High-resolution, live, directional mapping. *Heart Rhythm*. 2020;17:1621–1628.
4. Aksu T, Guler TE, Bozyel S, Yalin K. Usage of a new mapping algorithm to detect possible critical substrate for continuity of atrial fibrillation: fractionation mapping in preliminary experience. *J Interv Card Electrophysiol*. 2020;58:29–34.
5. Neuberger HR, Schotten U, Verheule S, Eijsbouts S, Blaauw Y, van Hunnik A, Allessie M. Development of a substrate of atrial fibrillation during chronic atrioventricular block in the goat. *Circulation*. 2005;111:30–37.
6. Mary-Rabine L, Albert A, Pham TD, Hordof A, Fenoglio JJ Jr, Malm JR, et al. The relationship of human atrial cellular electrophysiology to clinical function and ultrastructure. *Circ Res*. 1983;52:188–199.
7. Linzbach A. Heart failure from the point of view of quantitative anatomy. *Am J Cardiol*. 1960;5:370–382.
8. Saito T, Asai K, Sato S, Takano H, Mizuno K, Shimizu W. Ultrastructural features of cardiomyocytes in dilated cardiomyopathy with initially decompensated heart failure as a predictor of prognosis. *Eur Heart J*. 2015;36:724–732.